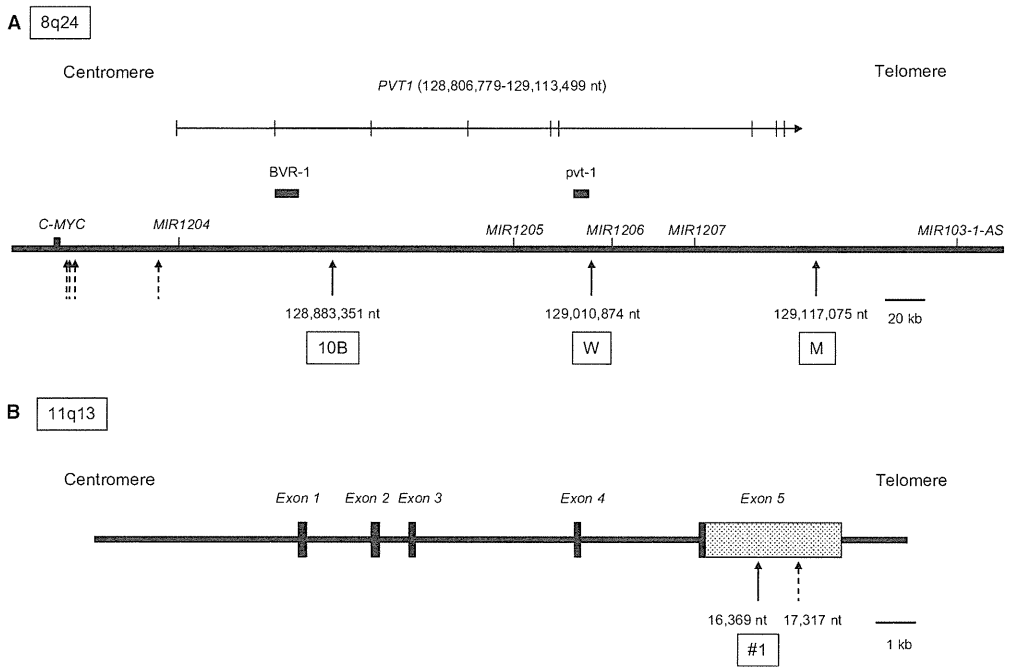

Figure 2 Distribution of 8q24 and 11q13 breakpoints. (A) Distribution of three 8q24 breakpoints in relation to *MYC*, *PVT1*, and previously determined breakpoints is illustrated. Two breakpoint cluster regions, BVR-1 (Burkitt's variant rearranged region) and pvt-1 (human counterpart of the murine plasmacytoma variant translocation 1 region), are shown as bars. The four dotted arrows indicate previously defined breakpoints of t(8;22)(q24;q11). The breakpoints are listed from left to right: BL37 (22), KK124 (23), BL2 (24), and patient 3 (27). 10B, W, and M in boxes represent the breakpoints of KHM10B, WILL2, and MD901, respectively. Nucleotide numbers are defined according to hg19. This figure is based on BLAT analysis and previous reports (6, 26). The structure of *PVT1* is based on the published sequence (Uc010mdq.3 Human Gene PVT1 306721). (B) Two breakpoints of der(11)t(11;22)(q13;q11) are in the 3'UTR of *CCND1*. Arrow indicates a breakpoint cloned in this study, whereas dotted arrow indicates a previous report (18). Solid boxes and dotted boxes indicate coding and non-coding regions, respectively.

The KHM2B cells showed one rearranged band probed with the IGLC1D fragment (Fig. 4A). The rearranged band was cloned using the lambda 1 primer set (Fig. 4A), and its nucleotide sequence was determined (accession no. AB724295). The rearrangement produced in-frame recombination between *IGLV2-14* and *IGLJ1* with 4-nucleotide insertion (ATGG) into the *Vλ/Jλ* junction. There were mutations in the variable region, with 91.2% match to the germ line (Fig. 4F).

In WILL2, two rearrangements, 12 and 4.6 kb, were found, using the IGLC3 probe on EcoR I blot (Fig. 4B). The 12-kb rearranged band theoretically represented t(8;22)(q24;q11). The 4.6-kb EcoRI fragment detected by Southern blot analysis was cloned by the lambda 3b primer set and sequenced (Fig. 4B). Although this cell line was established from a surface IGλ-positive tumor cell (8), this rearrangement resulted in an out-of-frame recombination between *V1-27P* and *IGLJ3* with insertion of the N-sequence (TGGG) (accession no. AB724296). The variable region showed a perfect match to the germ line (Fig. 4F).

KHM10B showed a 4.9-kb rearrangement of λ2 segment as well as a polymorphic band (Fig. 4C) on HindIII blot. The rearranged band was cloned by lambda 2b set primers (Fig. 4C). This rearrangement produced an in-frame recombination between *IGLV8-61* and *IGLJ3* with two overlapping nucleotides (TT) in the *Vλ–Jλ* junction (accession no. AB724297). The variable region showed 96.6% identity to the germ line (Fig. 4F).

In analyzing patient 2, we lacked Southern blot analysis data; therefore, all functional λ segments (λ1, λ2, λ3, and λ7) were examined by LDI-PCR. LDI-PCR using the lambda 1 primer set yielded a 4.2-kb DNA band of BglII digest, which differed from the germline band (11 kb) (Fig. 4D). Sequence analysis of the PCR product revealed that this rearrangement produced an in-frame recombination of *IGLV2-14* and *IGLJ1* with four N-sequences (ACTA) (accession no. AB724298). The variable region showed 97.6% identity to the germ line (Fig. 4F).

All LDI-PCR results were verified by conventional PCR using breakpoint-specific primers (Table S3 and Fig. 4E).

Discussion

Molecular analyses of *IG* genes, including Southern blot analysis, PCR, and FISH, in mature B-cell neoplasms provide useful diagnostic information. Southern blot analysis of

Figure 3 Nucleotide alignment encompassing breakpoints. (A) Junctional sequence of der(8)t(8;22)(q24;q11) of MD901. Bold letters indicate the first exon of *IGLL-5*. (B) Junctional sequence of der(8)t(8;22)(q24;q11) of WILL2. Bold and italics indicate *Jλ2* and N-nucleotide sequences, respectively. Underlined letters show 7-mer and 9-mer sequences of putative RRS. Italics indicate spacer (12 or 24 bp) sequence. (C) Junctional sequence of der(8)t(8;22)(q24;q11) of KHM10B. Bold letters indicate *Jλ3* sequence. Underlining shows 7-mer and 9-mer sequences separated with a spacer (indicated by italics). (D) Junctional sequence of der(11)t(11;22)(q13;q11) of patient 1. Bold letters indicate *Cλ7* sequence. Asterisks indicate nucleotide substitutions. 8, 22, and 11 indicate sequence derived from chromosome 8, 22, and 11, respectively. M, MD901; W, WILL2; 10B, KHM10B; and #1, patient 1.

IGλ can detect clonal rearrangement in many B-cell neoplasms; but, this method cannot distinguish *Vλ/Jλ* recombination or translocation. Conventional PCR can amplify *Vλ/Jλ* recombination setting *Vλ* and *Jλ* consensus sequence primers (19). Translocation breakpoints of t(3;22)(q27;q11) can be cloned by long-distance PCR (LD-PCR) (20) because most of the 3q27 break points are clustered in narrow regions, which makes primers setting adequate. If the breakpoints are separated widely, such as t(8;22)(q24;q11), appropriate primers for LD-PCR cannot be set. Moreover, conventional PCR cannot identify unknown translocation partners. Although chromosome analyses or FISH can detect chromosome translocation partner involving *IG* translocations (21, 22), these methods cannot determine nucleotide alignments of the breakpoints. The advantage of LDI-PCR is thus direct amplification of nucleotide alignment of unknown chromosome partners. Rapid molecular analysis of a small amount of DNA using LDI-PCR has been applied for rearrangements of *IGHJ*, *IGHS,* and *IGκ* (4–6). Together with our methods, almost all of *IG* rearrangements can be cloned by LDI-PCR, allowing us to understand the molecular events of *IG* genes in B-cell malignancies.

Three novel t(8;22)(q24;q11) were determined from two DLBCL (MD301 and WILL2) and one ALL-L3 (KHM10B) cell line. Some fraction of DLBCL, which harbors *MYC*/8q24 and other *IG* translocations concurrently, comprises most of the so-called double-hit lymphoma (DH lymphoma) (23). Indeed, the two DLBCL cell lines matched the criteria of DH lymphoma; MD901 and WILL2 represent *BCL6*$^+$/*MYC*$^+$ and *BCL2*$^+$/*MYC*$^+$ DH lymphoma, respectively. Although the clinicopathological significance of DH lymphoma has been well established, the mechanism and timing of multiple chromosome translocations seen in DH lymphoma are less clear. In *BCL6*$^+$/*MYC*$^+$ DH lymphoma, it is proposed that the both translocations are possibly mediated by the same mechanism in the germinal center (23). In MD901, t(3;22)(q27;q11) is thought to be a by-product of an erroneous recombination mediated by RAG1/2 because a RSS was found around the breakpoint (7). The t(8;22)(q24;q11) of this cell line, on the other hand, seems to arise from an unknown mechanism, using neither of erroneous *Vλ/Jλ* nor of SHM machineries, because the sequence around the breakpoint showed no RSS and very few nucleotide mutation. Interestingly, the *IGλ* break of this cell line is similar to that of a Burkitt cell line, BL37. The 22q11 breakpoint in MD901 fell to just 506 bp upstream of a previously cloned 22q11 breakpoint from BL37 (24). In addition, the t(8;22)(q24;q11) of BL37 is supposed to occur independently of the *Vλ/Jλ* and SMH processes (25), supporting our hypothesis on the origin of t(8;22)(q24;q11) in MD901. However, SHM may be found in a reciprocal breakpoint, as reported in Burkitt cell lines (KOBAK101 and LY91) with

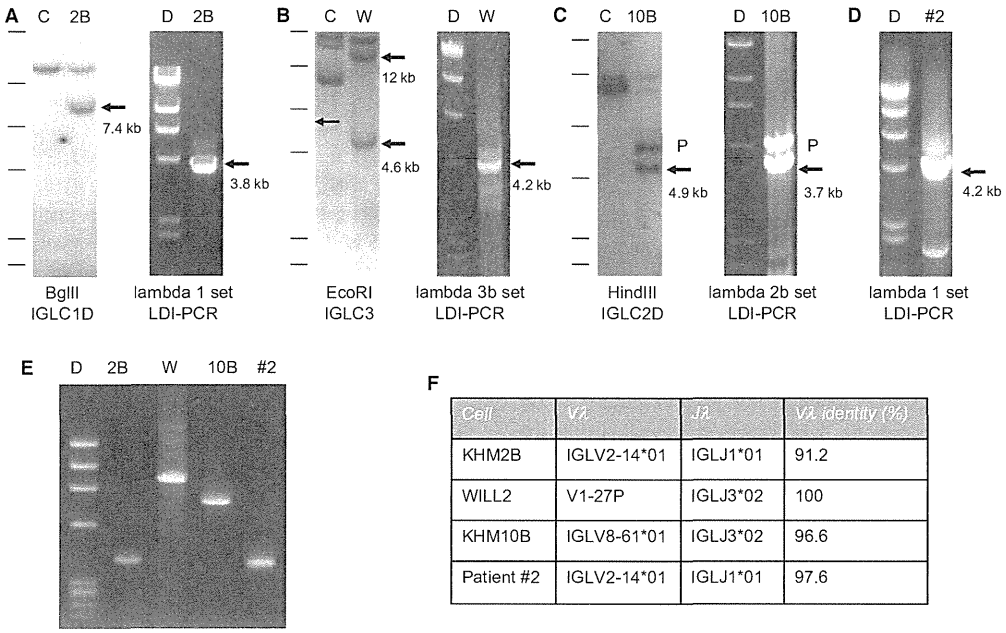

F

Cell	Vλ	Jλ	Vλ identity (%)
KHM2B	IGLV2-14*01	IGLJ1*01	91.2
WILL2	V1-27P	IGLJ3*02	100
KHM10B	IGLV8-61*01	IGLJ3*02	96.6
Patient #2	IGLV2-14*01	IGLJ1*01	97.6

Figure 4 Molecular cloning of *Vλ/Jλ* recombinations by LDI-PCR. (A) KHM2B showed one germline and another rearranged band (arrow) of *λ1* segment. The 7.4-kb rearranged band was amplified by LDI-PCR (arrow). (B) WILL2 showed two rearranged bands (arrows) on EcoRI blot probed with IGLC3. The 12-kb rearranged band was supposed to represent t(8;22)(q24;q11). The 4.6-kb rearranged band was amplified as a 4.2-kb PCR product. (C) KHM10B showed a polymorphic (indicated by P) and a rearranged band (arrow) on HindIII blot probed with IGLC2D. The rearranged band was cloned by LDI-PCR. (D) Patient 2 showed 4.2-kb PCR product (arrow) using lambda 1 primer set and BglII digest. (E) All LDI-PCR results were verified as expected PCR products using rearrangement-specific primers. 2B, W, 10B, #2, C, and D indicate KHM2B, WILL2, KHM10B, patient 2, germline control, and DNA marker (*λ*/HindIII and *ϕ*/HaeIII digest), respectively. (F) Sequence data of *Vλ/Jλ* recombination in each cell are summarized.

t(2;8)(p13;q24) (2, 26, 27). Therefore, analysis of the reciprocal breakpoint should explore detailed mechanism of t(8;22)(q24;q11) in the MD901. Overall, the sequence results obtained from the MD901 suggested that *BCL6*$^{+}$/*MYC*$^{+}$ can arise from a distinct mechanism. In *BCL2*$^{+}$/*MYC*$^{+}$ DH-lymphoma, it is suggested that the *BCL2* break is most probably mediated by RAG1/2 in precursor B cells in bone marrow and that *MYC*/8q24 break is a secondary event mediated by AID in the germinal center (23). The t(14;18)(q32;q13) of WILL2 showed a recombination between the major breakpoint region (MBR) of *BCL2* and J6 of *IGH* with RSS and N-nucleotide insertion (accession no. AB758553 in EMBL/GenBank/DDBJ databases), indicating that an aberrant *V(D)J* recombination mediated by RAG1/2 is responsible for this translocation. The t(8;22)(q24;q11) of this cell line also exhibited traces of a *Vλ/Jλ* recombination error, RSS, on both maternal chromosomes. Other characteristics of the *MYC*/8q24 break of this cell line are an insertion of 38 bp into the breakpoint junction and nucleotide mutation. As physiological *V/J* recombination in *IG* light chain genes is rarely associated N-nucleotide insertion (28), the 38-bp insertion might argue against involvement of a canonical *V/J* recombination. Also, the somatic mutation seen around the breakpoint might implicate SHM in the break. Taking the breakpoint analyses together, both t(14;18)(q32;q21) and t(8;22)(q24;q11) seen in WILL2 might be consequences of aberrant *V(D)J* recombinations; but, possible SMH involvement in t(8;22)(q24;q11) has not been ruled out. In t(8;14)(q24;q32) seen in BL, erroneous SHM or class switch recombination mediated by AID causes the translocation (29); however, in t(2;8)(p12;q24) or t(8;22)(q24;q11), the responsible mechanisms seem to be heterogeneous (25). Cloning data of t(8;22)(q24;q11) of the KHM10B suggested that this translocation would arise from *Vλ/Jλ* recombination mediated by RAG1/2, as the RSS found on both maternal chromosomes and no N-nucleotide insertion into the junction. To elucidate the mechanism and timing of t(8;22)(q24;q11) seen in DH lymphoma or BL, accumulation of cloning data, including both der(8) breakpoints and der(22) breakpoints, is warranted.

The 8q24 breakpoints of variant translocations at 3′ of *MYC* ranged up to 0.5 Mb downstream (6). Although 8q24 breakpoints are widespread, several putative breakpoint cluster regions have been proposed. The 8q24 break of the KHM10B fell to 20.2 and 14.8 kb downstream of that of BL64 and BL21, respectively. The breakpoint cluster of BL64, BL21, and LY91 is designed as BVR-1 (Burkitt's variants' rearranged region 1), which spans 11 kb (6, 26).

The breakpoint of the KHM10B might be associated with BVR-1. The 8q24 break of WILL2 is at just 2.0 kb 3′ of that of JBL2, which falls to the pvt-1 (the human counterpart of the murine plasmacytoma variant translocation 1 region) (27, 30). The 8q24 breakpoint of MD901 appears to have no association with previously reported cluster regions and is outside of *PVT1* region. It is not apparent whether EBV infection, histological type, or concurrent *IG* translocations affects the 8q24 breaks.

We determined *Vλ/Jλ* recombination sequences from four samples. Among them, the WILL2 result was unexpected. The cell line was established from CD10, CD19, CD20, and surface IGλ-positive DLBCL. It was thus anticipated that WILL2 had undergone a mutated but protein-coding *Vλ/Jλ* recombination. The cloning data, however, revealed that the allele showed no mutation and an out-of-fame recombination. This result indicated that protein-coding *Vλ/Jλ* recombination might be lost during *in vitro* culture.

Finally, many *IG* translocation partner genes have already been identified, but several uncloned *IGλ* translocations have been reported (21, 22). Our method is a useful tool for the identification of uncovered target genes involving the *IGλ* locus.

Acknowledgements

This work was supported by a grant (no. 18591082) from the Ministry of Education, Culture, Sports, Science, and Technology (MEXT), Japan.

Authorship

Contributions: M.S. and T.S. designed this work; M.S., H. H., J. W., and T.S. performed Southern blot analysis; M.S., H.H., J. W., S. M., and T.S. performed PCR; K. K. analyzed patient no.1; M.S., H. M., N. H., T.S and H. N., wrote the manuscript.

Conflict of interest disclosure

All authors declare no competing financial interests.

References

1. Willis TG, Dyer MJ. The role of immunoglobulin translocations in the pathogenesis of B-cell malignancies. *Blood* 2000;**96**:808–22.
2. Küppers R, Dalla-Favera R. Mechanisms of chromosomal translocations in B cell lymphomas. *Oncogene* 2001;**20**:5580–94.
3. Shaffer AL, Rosenwald A, Staudt LM. Lymphoid malignancies: the dark side of B-cell differentiation. *Nat Rev Immunol* 2002;**2**:920–32.
4. Willis TG, Jadayel DM, Coignet LJ, Abdul-Rauf M, Treleaven JG, Catovsky D, Dyer MJ. Rapid molecular cloning of rearrangements of the IGHJ locus using long-distance inverse polymerase chain reaction. *Blood* 1997;**90**:2456–64.
5. Sonoki T, Willis TG, Oscier DG, Karran EL, Siebert R, Dyer MJ. Rapid amplification of immunoglobulin heavy chain switch (IGHS) translocation breakpoints using long-distance inverse PCR. *Leukemia* 2004;**18**:2026–31.
6. Kroenlein H, Schwartz S, Reinhardt R, Rieder H, Molkentin M, Gökbuget N, Hoelzer D, Thiel E, Burmeister T. Molecular analysis of the t(2;8)/MYC-IGK translocation in high-grade lymphoma/leukemia by long-distance inverse PCR. *Genes Chromosom Cancer* 2012;**51**:290–9.
7. Miki T, Kawamata N, Arai A, Ohashi K, Nakamura Y, Kato A, Hirosawa S, Aoki N. Molecular cloning of the breakpoint for 3q27 translocation in B-cell lymphomas and leukemias. *Blood* 1994;**83**:217–22.
8. Sonoki T, Li Y, Miyanishi S, Nakamine H, Hanaoka N, Matsuoka H, Mori I, Nakakuma H. Establishment of a novel CD20 negative mature B-cell line, WILL2, from a CD20 positive diffuse large B-cell lymphoma patient treated with rituximab. *Int J Hematol* 2009;**89**:400–2.
9. Sonoki T, Matsuzaki H, Miyamoto K, *et al.* Establishment of the novel B acute lymphoblastic leukemia (FAB L3) cell line KHM-10B with a 13q34 abnormality and constitutive expression of c-myc and max during cell cycle. *Leukemia* 1995;**9**:2093–9.
10. Matsuzaki H, Hata H, Asou N, Suzushima H, Akahoshi Y, Yoshida M, Nagakura S, Ishii T, Sanada I, Takatsuki K. Establishment and characterization of acute B-cell lymphocytic leukemia cell line showing (8;14) and (14;18) chromosome translocation. *Acta Haematol* 1990;**84**:156–61.
11. Kawakami K, Miyanishi S, Sonoki T, Nakamura S, Nomura K, Taniwaki M, Murata T, Kadowaki S, Kadowaki N, Miura I. Case of B-cell lymphoma with rearrangement of the BCL1, BCL2, BCL6, and c-MYC genes. *Int J Hematol* 2004;**79**:474–9.
12. Sonoki T, Harder L, Horsman DE, *et al.* Cyclin D3 is a target gene of t(6;14)(p21.1;q32.3) of mature B-cell malignancies. *Blood* 2001;**98**:2837–44.
13. Tümkaya T, Comans-Bitter WM, Verhoeven MA, Van Dongen JJ. Southern blot detection of immunoglobulin lambda light chain gene rearrangements for clonality studies. *Leukemia* 1995;**9**:2127–32.
14. Tümkaya T, Beishuizen A, Wolvers-Tettero IL, Van Dongen JJ. Identification of immunoglobulin lambda isotype gene rearrangements by Southern blot analysis. *Leukemia* 1996;**10**:1834–9.
15. Altschul SF, Gish W, Miller W, Myers EW, Lipman DJ. Basic local alignment search tool. *J Mol Biol* 1990;**215**:403–10.
16. Fujita PA, Rhead B, Zweig AS, *et al.* The UCSC Genome Browser database: update 2011. *Nucleic Acids Res* 2011;**39** (Database issue):D876–82.
17. Merelli I, Guffanti A, Fabbri M, Cocito A, Furia L, Grazini U, Bonnal RJ, Milanesi L, McBlane F. RSSsite: a reference database and prediction tool for the identification of cryptic Recombination Signal Sequences in human and murine

genomes. *Nucleic Acids Res* 2010;**38**(Web Server issue): W262–7.
18. Komatsu H, Iida S, Yamamoto K, Mikuni C, Nitta M, Takahashi T, Ueda R, Seto M. A variant chromosome translocation at 11q13 identifying PRAD1/cyclin D1 as the BCL-1 gene. *Blood* 1994;**84**:1226–31.
19. Sahota SS, Babbage G, Zojer N, Ottensmeier CH, Stevenson FK. Determining mutational status of immunoglobulin v genes in chronic lymphocytic leukemia: a useful prognostic indicator. *Methods Mol Med* 2005;**115**:129–44. Eds by Illidge T and Johnson PWM.
20. Akasaka H, Akasaka T, Kurata M, Ueda C, Shimizu A, Uchiyama T, Ohno H. Molecular anatomy of BCL6 translocations revealed by long-distance polymerase chain reaction-based assays. *Cancer Res* 2000;**60**:2335–41.
21. Martőn-Subero JI, Harder L, Gesk S, Schlegelberger B, Grote W, Martinez-Climent JA, Dyer MJ, Novo FJ, Calasanz MJ, Siebert R. Interphase FISH assays for the detection of translocations with breakpoints in immunoglobulin light chain loci. *Int J Cancer* 2002;**98**:470–4.
22. Fujimoto Y, Nomura K, Fukada S, *et al.* Immunoglobulin light chain gene translocations in non-Hodgkin's lymphoma as assessed by fluorescence *in situ* hybridisation. *Eur J Haematol* 2008;**80**:143–50.
23. Aukema SM, Siebert R, Schuuring E, Van Imhoff GW, Kluin-Nelemans HC, Boerma EJ, Kluin PM. Double-hit B-cell lymphomas. *Blood* 2011;**117**:2319–31.
24. Hollis GF, Mitchell KF, Battey J, Potter H, Taub R, Lenoir GM, Leder P. A variant translocation places the lambda immunoglobulin genes 3′ to the c-myc oncogene in Burkitt's lymphoma. *Nature* 1984;**307**:752–5.
25. Cario G, Stadt UZ, Reiter A, Welte K, Sykora KW. Variant translocations in sporadic Burkitt's lymphoma detected in fresh tumour material: analysis of three cases. *Br J Haematol* 2000;**110**:537–46.
26. Kato S, Tachibana K, Takayama N, Kataoka H, Yoshida MC, Takano T. Genetic recombination in a chromosomal translocation t(2;8)(p11;q24) of a Burkitt's lymphoma cell line, KOBK101. *Gene* 1991;**97**:239–44.
27. Henglein B, Synovzik H, Groitl P, Bornkamm GW, Hartl P, Lipp M. Three breakpoints of variant t(2;8) translocations in Burkitt's lymphoma cells fall within a region 140 kilobases distal from c-myc. *Mol Cell Biol* 1989;**9**: 2105–13.
28. Yancopoulos GD, Alt FW. Regulation of the assembly and expression of variable-region genes. *Annu Rev Immunol* 1986;**4**:339–68.
29. Guikema JE, Schuuring E, Kluin PM. Structure and consequences of IGH switch breakpoints in Burkitt lymphoma. *J Natl Cancer Inst Monogr* 2008;**39**:32–6.
30. Graham M, Adams JM. Chromosome 8 breakpoint far 3′ of the c-myc oncogene in a Burkitt's lymphoma 2;8 variant translocation is equivalent to the murine pvt-1 locus. *EMBO J* 1986;**5**:2845–51.

Supporting Information

Additional Supporting Information may be found in the online version of this article:

Figure S1. (A) Enzyme map of *IGλ* locus, isotype-specific probes and positions of primer sets. This figure is based on a previous report (14) and published sequence data (accession no. X51755 and NG_000002). B: BamHI, E: EcoRI, G: BglII, H: HindIII, S: SphI, and T: TaqI. The IGLJ2 probe recognizes both λ 2 and λ 3 segments (indicated by an asterisk). IGLC2D contains an SphI site. Arrowheads indicate primer pairs. (B) Schema of deregulation of the partner gene by *IGλ* translocation is illustrated. The partner gene is affected by *IGλ* from telomeric sides. (C) Germline fragments of eachλ segment can be amplified by LDI-PCR using respective primer sets. 1: λ1 (11 kb of Bgl II fragment amplified with lambda 1 primer set), 2: λ2 (8.1 kb of Hind III fragment amplified with lambda 2a primer set), 3: λ2 (7.8 kb of Hind III fragment amplified with lambda 2b primer set), 4: λ3 (3.7 kb of Taq I fragment amplified with lambda 3a primer set), 5: λ3 (4.1 kb of Taq I fragment amplified with lambda 3b primer set), 6: λ4 (3.5 kb of BamH I fragment amplified with lambda 4 primer set), 7: λ5 (4.4 kb of Bgl II fragment amplified with lambda 5 primer set), 8: λ6 (4.4 kb of BamH I fragment amplified with lambda 6 primer set), 9: λ7 (1.9 kb of BamH I fragment with lambda 7 primer set). D: DNA marker (λ/HindIII and λ/HaeIII digest).

Table S1. Primers for LDI-PCR.

Table S2. DNA size of germ line fragment.

Table S3. Primers for verification.

References

Chou, T.C. & Talalay, P. (1984) Quantitative analysis of dose-effect relationships: the combined effects of multiple drugs or enzyme inhibitors. *Advances in Enzyme Regulation*, **22**, 27–55.

Fahy, B.N., Schlieman, M.G., Virudachalam, S. & Bold, R.J. (2003) Schedule-dependent molecular effects of the proteasome inhibitor bortezomib and gemcitabine in pancreatic cancer. *Journal of Surgical Research*, **113**, 88–95.

Lonial, S., Kaufman, J., Tighiouart, M., Nooka, A., Langston, A.A., Heffner, L.T., Torre, C., McMillan, S., Renfroe, H., Harvey, R.D., Lechowicz, M.J., Khoury, H.J., Flowers, C.R. & Waller, E.K. (2010) A phase I/II trial combining high-dose melphalan and autologous transplant with bortezomib for multiple myeloma: a dose- and schedule-finding study. *Clinical Cancer Research*, **16**, 5079–5086.

Mitsiades, N., Mitsiades, C.S., Richardson, P.G., Poulaki, V., Tai, Y.T., Chauhan, D., Fanourakis, G., Gu, X., Bailey, C., Joseph, M., Libermann, T. A., Schlossman, R., Munshi, N.C., Hideshima, T. & Anderson, K.C. (2003) The proteasome inhibitor PS-341 potentiates sensitivity of multiple myeloma cells to conventional chemotherapeutic agents: therapeutic applications. *Blood*, **101**, 2377–2380.

Nencioni, A., Hua, F., Dillon, C.P., Yokoo, R., Scheiermann, C., Cardone, M.H., Barbieri, E., Rocco, I., Garuti, A., Wesselborg, S., Belka, C., Brossart, P., Patrone, F. & Ballestrero, A. (2005) Evidence for a protective role of Mcl-1 in proteasome inhibitor-induced apoptosis. *Blood*, **105**, 3255–3262.

Popat, R., Oakervee, H., Williams, C., Cook, M., Craddock, C., Basu, S., Singer, C., Harding, S., Foot, N., Hallam, S., Odeh, L., Joel, S. & Cavenagh, J. (2009) Bortezomib, low-dose intravenous melphalan, and dexamethasone for patients with relapsed multiple myeloma. *British Journal of Haematology*, **144**, 887–894.

San Miguel, J.F., Schlag, R., Khuageva, N.K., Dimopoulos, M.A., Shpilberg, O., Kropff, M., Spicka, I., Petrucci, M.T., Palumbo, A., Samoilova, O.S., Dmoszynska, A., Abdulkadyrov, K.M., Schots, R., Jiang, B., Mateos, M.V., Anderson, K.C., Esseltine, D.L., Liu, K., Cakana, A., van de Velde, H. & Richardson, P.G. (2008) Bortezomib plus melphalan and prednisone for initial treatment of multiple myeloma. *New England Journal of Medicine*, **359**, 906–917.

Spanswick, V.J., Craddock, C., Sekhar, M., Mahendra, P., Shankaranarayana, P., Hughes, R.G., Hochhauser, D. & Hartley, J.A. (2002) Repair of DNA interstrand crosslinks as a mechanism of clinical resistance to melphalan in multiple myeloma. *Blood*, **100**, 224–229.

Weigert, O., Pastore, A., Rieken, M., Lang, N., Hiddemann, W. & Dreyling, M. (2007) Sequence-dependent synergy of the proteasome inhibitor bortezomib and cytarabine in mantle cell lymphoma. *Leukemia*, **21**, 524–528.

Yarde, D.N., Oliveira, V., Mathews, L., Wang, X., Villagra, A., Boulware, D., Shain, K.H., Hazlehurst, L.A., Alsina, M., Chen, D.T., Beg, A.A. & Dalton, W.S. (2009) Targeting the Fanconi anemia/BRCA pathway circumvents drug resistance in multiple myeloma. *Cancer Research*, **69**, 9367–9937.

Occupancy of whole blood cells by a single *PIGA*-mutant clone with *HMGA2* amplification in a paroxysmal nocturnal haemoglobinuria patient having blood cells with NKG2D ligands

Paroxysmal nocturnal haemoglobinuria (PNH) is an acquired stem cell disorder caused by expansion of PNH clones that harbour *PIGA* mutations and lack glycosylphosphatidylinositol (GPI)-linked membrane proteins, such as CD55 and CD59, leading to complement-mediated intravascular haemolysis and thrombosis (Parker & Ware, 2003). PNH also manifests immune-mediated bone marrow (BM) failure. PNH presents critical problems that need to be resolved (Luzzatto *et al*, 1997; Dunn *et al*, 2000; Inoue *et al*, 2003; Nakakuma & Kawaguchi, 2003; Parker & Ware, 2003): the mechanism by which PNH clones expand, the pathogenesis of BM failure, which is a major cause of death, and PNH aetiology.

Two hypotheses exist for the mechanism of clonal expansion: survival and growth advantage theories. For the first theory, PNH clones selectively survive in the setting of immune-mediated BM injury (survival advantage) (Dunn *et al*, 2000; Inoue *et al*, 2003; Nakakuma & Kawaguchi, 2003). A possible candidate for this is NKG2D (KLRK1)-mediated immunity (Hanaoka *et al*, 2009), which is triggered by the expression of ligands, such as major histocompatibilty complex class I chain-related peptides A and B (MICA/B) and cytomegalovirus UL-16 binding proteins (ULBPs). MICA/B and ULBPs are peptide-linked (transmembrane) and GPI-linked membrane proteins, respectively. The ligands share NKG2D as a common receptor on such lymphocytes as natural killer (NK) cells and $CD8^+$ cytotoxic T cells. The engagement of NKG2D with its ligands that are frequently coexpressed promotes the elimination of NKG2D ligand-expressing cells by $NKG2D^+$ lymphocytes. Then, PNH clones lacking GPI-linked ULBPs may preferentially survive by immunoselection (Hanaoka *et al*, 2006). The growth advantage theory is partly supported by the pathological expression of genes such as high mobility group AT-hook 2 (*HMGA2*), which encodes a transcription factor often found in benign tumours such as lipoma and myoma, early growth response factor 1 (*EGR1*), and Wilms' tumour 1 (*WT1*) (Inoue *et al*, 2003; Nakakuma & Kawaguchi, 2003; Ikeda *et al*, 2011;

Murakami *et al*, 2012). Current reports suggest that the two theories are cooperative rather than mutually exclusive (Inoue *et al*, 2003; Nakakuma & Kawaguchi, 2003). Indeed, we here report a patient with PNH showing this cooperation.

A 47-year-old woman was diagnosed as having PNH with a coexisting congenital deficiency of C9 in 1980. She is presently 79 years old and has maintained a high quality of life for more than 32 years after PNH diagnosis. She has mild BM failure responsive to low-dose metenolone acetate (10 mg/day). She also manifests very low levels of both intra- and extravascular haemolysis, with detection of haemosiderinuria and C3d-bound erythrocytes (Hanaoka *et al*, 2012). Flow cytometry showed complete occupancy of her peripheral blood by PNH cells negative for both CD55 and CD59 (Fig 1A). Erythrocytes (Fig 1B) and leucocytes (Fig 1C) all had the PNH phenotype. In general, it is very rare that all lymphocytes show PNH phenotype even in patients with high population of PNH-erythrocytes and -granulocytes. Of interest, virtually all cells in the lymphocyte fraction ($CD11b^-$ leucocytes) were also negative for CD55 and CD59 (Fig 1C). It is then conceivable that all haematopoietic stem cells are also affected. The blood cells were of a single *PIGA*-mutant clone, which has persistently maintained haematopoiesis under the treatment with low-dose metenolone acetate for more than 13 years since 1998 (data not shown). These findings prompted us to be concerned about the mechanism by which the mutant clone completely occupies blood cells in the patient.

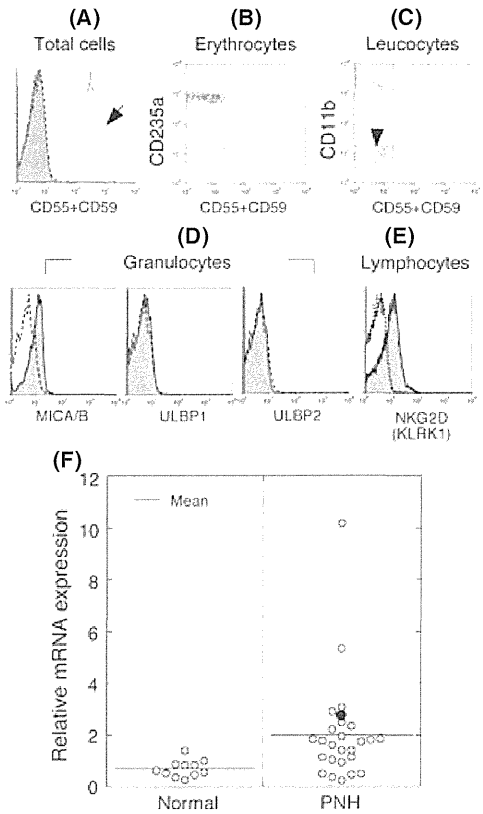

Fig 1. Characterization of the PNH clone. (**A-C**) Lack of CD55 and CD59. (**A**) total peripheral blood cells (Total cells, shaded histogram), (**B**) erythrocytes ($CD235a^+$ cells), (**C**) granulocytes ($CD11b^+$ cells) and lymphocytes ($CD11b^-$ cells, ▼). An arrow (in panel **A**) indicates blood cells positive for CD55 and CD59 of a healthy donor (positive control). (**D**) Granulocytes positive for MICA/B but negative for ULBPs. (**E**) Lymphocytes positive for NKG2D. (**F**) *HMGA2* mRNA amplification in leucocytes of the present case in this report. For comparison, the data of the present case (•) were shown together with our published data of 25 patients with PNH (PNH) and 11 healthy volunteers (Normal) (Murakami *et al*, 2012). The value of relative expression shows the ratio of *HMGA2* mRNA expression: sample/normal control. The mean relative mRNA expression (—) was 1·97 ± 1·15 (standard deviation, SD) in PNH, 2·73 in the present case of PNH, and 0·70 ± 0·26 in normal individuals. (**A**, **D**, and **E**) Dotted lines in the histograms indicate nonspecific background staining with isotype-matched control immunoglobulin.

Regarding NKG2D-mediated immunity as a potential candidate that allows the immunoselection of PNH clones (Inoue *et al*, 2003; Nakakuma & Kawaguchi, 2003; Hanaoka *et al*, 2006, 2009), we confirmed the pathological expression of MICA/B, peptide-linked NKG2D ligands, on granulocytes (Fig 1D). Given that NKG2D receptor is expressed in the patient's lymphocytes (Fig 1E), NKG2D-mediated injury of the blood cells may occur in the patient (Hanaoka *et al*, 2006, 2009). In this setting, the *PIGA*-mutant clone lacking ULBPs as GPI-linked NKG2D ligands (Fig 1D) may survive and accumulate (Hanaoka *et al*, 2006, 2009), leading to clonal expansion. Of note, the *PIGA*-mutant clone also showed *HMGA2* amplification about four times normal (Fig 1F), which is reported to confer the benign tumour-like growth phenotype (Ikeda *et al*, 2011; Murakami *et al*, 2012). The amplification may also support expansion of the mutant clone in the patient.

This is the first case of PNH indicating the marked expansion of a single PNH clone by combination of both survival and growth advantages.

Acknowledgements

The authors thank Tatsuya Kawaguchi of Kumamoto University for his critical discussion.

This work was supported by grants from the Ministry of Education, Culture, Sports, Science, and Technology of Japan, the Ministry of Labour and Welfare of Japan, and the Takeda Science Foundation.

Author contributions

NH designed and performed research, analysed data, and wrote the paper. YM and TK performed molecular analyses. MN, KH, SN, YY, SM, and TS analysed clinical data. HN supervised the project, analysed data, and wrote the paper.

Conflicts of interest

All authors declare no competing financial interests.

Nobuyoshi Hanaoka[1]
Yoshiko Murakami[2]
Masahide Nagata[3]
Kentaro Horikawa[4]
Shoichi Nagakura[5]
Yuji Yonemura[6]
Shogo Murata[1]
Takashi Sonoki[1]
Taroh Kinoshita[2]
Hideki Nakakuma[1]
[1]*Department of Haematology/Oncology, Wakayama Medical University, Wakayama,* [2]*Research Institute for Microbial Diseases and WPI Immunology Frontier Research Centre, Osaka University, Osaka,* [3]*Nagata ENT Clinic, Kumamoto,* [4]*Koshi Dai-Ichi Hospital, Kumamoto,* [5]*Department of Haematology, National Hospital Organization Kumamoto Medical Centre, Kumamoto, and* [6]*Department of Blood Transfusion Medicine and Cell Therapy, Kumamoto University, Kumamoto, Japan*
E-mail: nhanaoka@wakayama-med.ac.jp

Keywords: paroxysmal nocturnal haemoglobinuria, immunoselection, clonal expansion, NKG2D (KLRK1), high mobility group AT-hook 2

First published online 18 October 2012
doi: 10.1111/bjh.12093

References

Dunn, D.E., Liu, J.M. & Young, N.S. (2000) Paroxysmal nocturnal hemoglobinuria. In: *Bone Marrow Failure Syndromes* (ed. by N.S. Young), pp. 99–121. Saunders, Philadelphia, PA.

Hanaoka, N., Kawaguchi, T., Horikawa, K., Nagakura, S., Mitsuya, H. & Nakakuma, H. (2006) Immunoselection by natural killer cells of *PIGA* mutant cells missing stress-inducible ULBP. *Blood*, **107**, 1184–1191.

Hanaoka, N., Nakakuma, H., Horikawa, K., Nagakura, S., Tsuzuki, Y., Shimanuki, M., Kojima, K., Yonemura, Y. & Kawaguchi, T. (2009) NKG2D-mediated immunity underlying paroxysmal nocturnal haemoglobinuria and related bone marrow failure syndromes. *British Journal of Haematology*, **146**, 538–545.

Hanaoka, N., Murakami, Y., Nagata, M., Nagakura, S., Yonemura, Y., Sonoki, T., Kinoshita, T. & Nakakuma, H. (2012) Persistently high quality of life conferred by coexisting congenital deficiency of terminal complement C9 in a paroxysmal nocturnal hemoglobinuria patient. *Blood*, **119**, 3866–3868.

Ikeda, K., Mason, P.J. & Bessler, M. (2011) 3'UTR-truncated *Hmga2* cDNA causes MPN-like hematopoiesis by conferring a clonal growth advantage at the level of HSC in mice. *Blood*, **117**, 5860–5869.

Inoue, N., Murakami, Y. & Kinoshita, T. (2003) Molecular genetics of paroxysmal nocturnal hemoglobinuria. *International Journal of Hematology*, **77**, 107–112.

Luzzatto, L., Bessler, M. & Rotoli, B. (1997) Somatic mutations in paroxysmal nocturnal hemoglobinuria: a blessing in disguise? *Cell*, **88**, 1–4.

Murakami, Y., Inoue, N., Shichishima, T., Ohta, R., Noji, H., Maeda, Y., Nishimura, J., Kanakura, Y. & Kinoshita, T. (2012) Deregulated expression of *HMGA2* is implicated in clonal expansion of *PIGA* deficient cells in paroxysmal nocturnal haemoglobinuria. *British Journal of Haematology*, **156**, 383–387.

Nakakuma, H. & Kawaguchi, T. (2003) Pathogenesis of selective expansion of PNH clones. *International Journal of Hematology*, **77**, 121–124.

Parker, C.J. & Ware, R.E. (2003) Paroxysmal nocturnal hemoglobinuria. In: *Wintrobe's Clinical Hematology* (ed. by J.P. Greer, F. Foerster, J.N. Leukens, G.M. Rodgers, F. Paraskevas & B. Glader), pp. 1203–1221. Lippincott Williams and Wilkins, Baltimore, MD.

Complement C3 is a substrate for activated factor XIII that is cross-linked to fibrin during clot formation

Complement C3 is the main effector protein of the complement system and plays a major role in innate immunity. A growing body of evidence indicates complex interactions between the complement and coagulation cascades (Oikonomopoulou *et al*, 2012), which are likely to be beneficial in the context of protection following injury. We previously identified C3 as a novel clot component and demonstrated that C3 binds to fibrin with high affinity and prolongs fibrinolysis in a purified system and plasma milieu (Howes *et al*, 2012), consistent with results of several clinical studies (Schroeder *et al*, 2010; Hess *et al*, 2012; Howes *et al*, 2012).

In the present study we further explored the mechanisms by which C3 becomes incorporated into clots, by evaluating the interactions between C3 and factor XIII (FXIII). Using 5-(biotinamido)pentylamine (BPNH2) in microplate-based cross-linking assays (full details of all methods are provided Appendix S1), BPNH2 was incorporated into immobilized C3 and fibrinogen (positive control) in the presence of thrombin-activated FXIII (FXIIIa) but not zymogen FXIII (FXIIIA2B2) in a concentration-dependent manner (Fig 1A). Time-dependent incorporation of BPNH2 to C3 in the fluid phase was also observed in the presence of FXIIIa but not

Open

Leukemia (2013) **27,** 233–258

www.nature.com/leu

LETTERS TO THE EDITOR

Pretreatment of leukemic cells with low-dose decitabine markedly enhances the cytotoxicity of gemtuzumab ozogamicin

Leukemia (2013) **27,** 233–235; doi:10.1038/leu.2012.178

Prognosis in relapsed/refractory acute myeloid leukemia (AML) is poor due to drug resistance. Gemtuzumab ozogamicin (GO) is a molecularly targeted drug, which consists of anti-CD33 antibody and calicheamicin. The high expression of CD33 antigen on most AML cells and exceptionally marked cytotoxicity of calicheamicin have attracted strong interest in GO, but clinical results on GO monotherapy have been disappointing, and methods of overcoming resistance to GO have accordingly been sought.

GO requires several cellular steps to exert its effect, including expression of the CD33 antigen, internalization of the CD33–GO complex into the cell, linker digestion in lysosomes and inter-

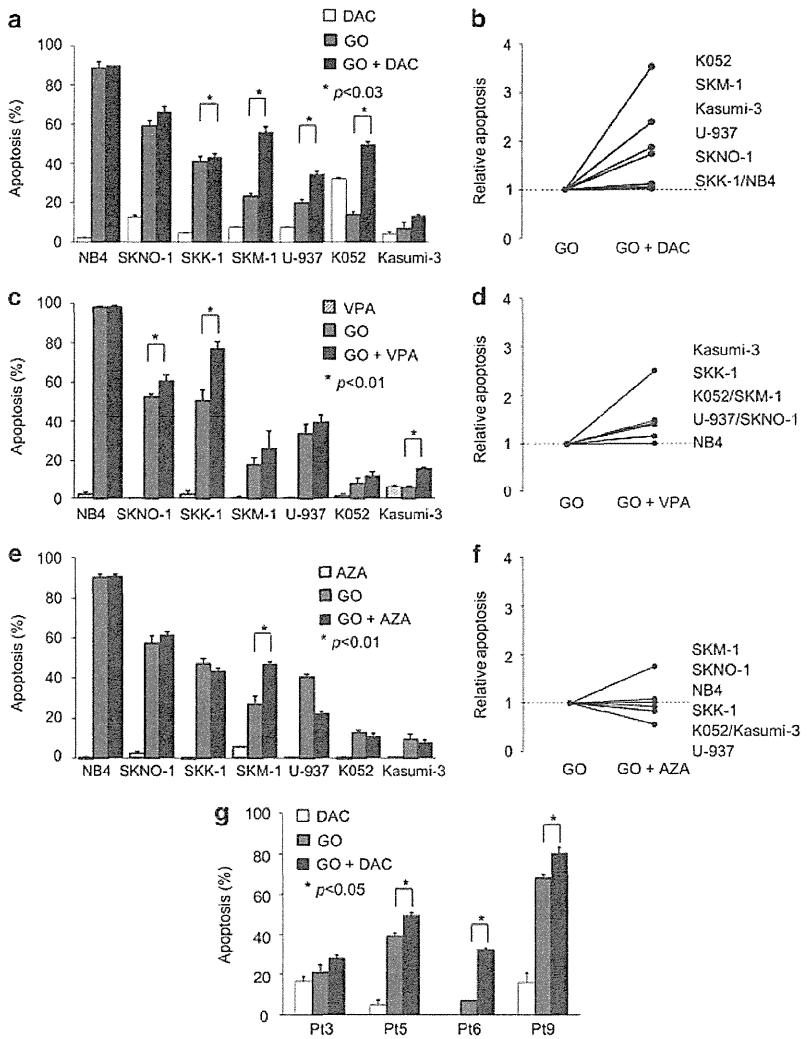

Figure 1. Combination effect of GO with DAC, VPA or AZA in CD33-positive leukemic cells. Cells were treated with 100 nM DAC (**a**, **b**, **g**), 1 mM VPA (**c**, **d**) or 2 μM AZA (**e**, **f**) for 48 h before GO (2.5 μg/ml) administration, cultured for an additional 24 h, and then apoptosis was measured. Apoptotic cells (%) increased in SKNO-1, SKK-1, SKM-1, U-937 and K052 cells when combined with DAC (**a**), in SKNO-1, SKK-1 and Kasumi-3 cells when combined with VPA (**c**) and in SKM-1 cells when combined with AZA (**e**). (**b**, **d**, **f**) Cell lines show relative apoptosis, namely apoptotic cells (%) in combination/apoptotic cells (%) in single GO administration, with any number > 1 indicating a combination effect versus any number < 1 meaning no combination effect. Combination of GO and DAC was superior in both the number of cell lines impacted and mean relative apoptosis. (**g**) Combination effect of GO with DAC was seen in four cells among 14 cells from patients with refractory AML. The degree of effect varied widely.

Accepted article preview online 3 July 2012; advance online publication, 20 July 2012

calation of calicheamicin into DNA (Supplementary Figure S1).[1,2] The exertion of cytotoxicity thus requires that these target cell functions remain intact. Some of these cellular functions may be characteristically suppressed in refractory leukemic cells, or downgraded by the combined chemotherapy. We therefore speculated that the use of an agent that amplifies the cellular functions necessary for GO's action would extract its essential efficacy.

In AML or myelodysplastic syndrome, epigenetic alterations of methylation or acetylation are considered to be associated with disease cause.[3–5] In low concentrations, the purine analogs decitabine (DAC) and azacitidine (AZA) act mainly to inhibit DNA methyltransferase rather than to induce cell death,[3,4] and have therefore been speculated to improve epigenetic deterioration.[3,4,6,7] The histone deacetylase inhibitor valproic acid (VPA) is also expected to improve epigenetic deterioration,[8,9] and has been reported to intensify the cytotoxic effect of GO.[10]

Accordingly, we considered that strengthening the activity of GO might be better achieved by taking advantage of epigenetic-modulating agents such as DAC, VPA and AZA, rather than by the simple combination of strongly cytotoxic drugs. Here, we report the use of pretreatment with DAC to augment the efficacy of GO.

We first evaluated the cytotoxic effect of GO, DAC, VPA and AZA as single agents in various leukemic cell lines (Supplementary Figure S2). GO induced strong apoptosis in NB4 cells derived from an acute promyelocytic leukemia patient. The other cell lines, most of them were derived from refractory patients, were less sensitive to GO, including AML/MRC-derived lines (SKK-1 cells and SKM-1 cells), complex karyotype AML cells (SKNO-1, K052 and Kasumi-3) and a myelomonocytic leukemia line (U-937) (Supplementary Figure S2). DAC, VPA or AZA revealed scant cytotoxicity in any of these cells.

We next investigated whether the cytotoxic effect of GO was enhanced on combination with these three agents. We first combined GO and DAC. As no combination effect was seen when GO and DAC were administered simultaneously (data not shown), we evaluated a change in timing of DAC administration from 12, 24, 48 and 72 h before the administration of GO and 12 h after. A degree of combination effect was observed at every point that DAC was administered before GO, which was maximal at 48 h before GO (data not shown). Pretreatment with DAC enhanced sensitivity to GO in all GO-resistant AML cells (Figure 1a). The degree of combination effect varied among cell lines (Figure 1b); in particular, pretreatment in K052 and SKM-1 cells demonstrated a greater than twofold increase in cytotoxic effect compared with GO alone (Figure 1b). We next analyzed the combinational effects of VPA (Figures 1c and d) and AZA (Figures 1e and f) with GO. Similar to DAC, AZA produced a combination effect only when administered before GO, whereas concurrent administration of VPA and GO did show a combination effect. Among the seven cell lines analyzed, a combination effect was observed in four cell lines with DAC, three with VPA and one with AZA, with mean relative increases in apoptosis of 2.02, 1.87 and 1.27, respectively. These findings clearly show that pretreatment with DAC provided the greatest increase in effect of GO, and suggest that DAC may have some effect in overcoming resistance to GO.

To confirm the enhancement in freshly-isolated cells, primary leukemic cells obtained from patients with refractory AML were treated *in vitro* with DAC following GO, and the degree of apoptosis was measured (Figure 1g). A combination effect of DAC and GO on apoptosis was observed in four of 14 patients (29%). The degree of combination effect differed widely. This result suggested that ~30% of patients with poor outcomes under conventional therapy might expect some effect by this combination.

We then investigated the mechanism by which DAC overcomes resistance to GO, along with the putative steps of action of GO (Supplementary Figure S1). We first measured the expression level of CD33 antigen in each cell line, and then assessed the degree

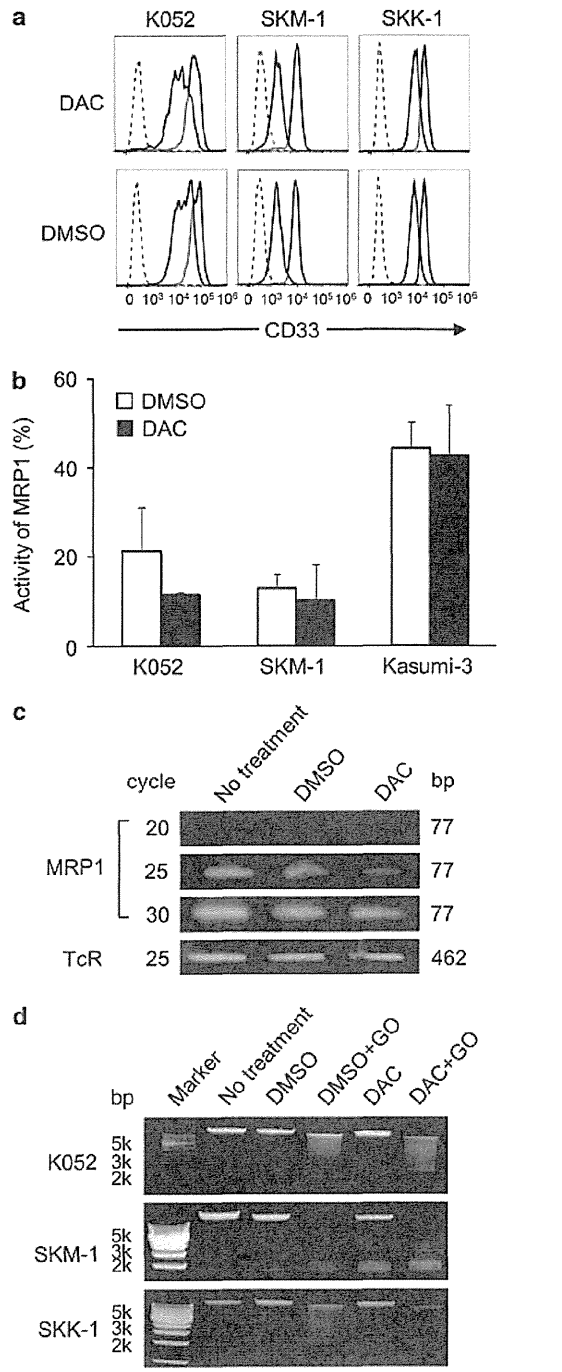

Figure 2. Points of action of the pretreatment effect of DAC. (**a**) Change in the expression of CD33 antigen was measured with a flow cytometer. CD33 antigen expression (MFI) was decreased after 4-h incubation with anti-CD33 antibody (shaded curves). Dotted curves represent isotype controls. (**b**, **c**) Activity and mRNA expression of MRP1 with or without DAC treatment. MRP1 activity was reduced by DAC treatment in K052 cells, whereas no change was seen in SKM-1 or Kasumi-3 cells (**b**). mRNA expression of MRP1 was reduced by DAC treatment in K052 cells (**c**). (**d**) DNA fragmentation by GO was enhanced by DAC pretreatment in K052 and SKM-1 cells. DAC pretreatment produced no increase in DNA fragmentation by GO in SKK-1 cells.

of internalization. Cell surface expression of CD 33 antigen was seen in all cell lines (Figure 2a, solid lines; only data of K052, SKM-1 and SKK-1 are indicated). No difference in CD33 expression was seen before and after pretreatment with DAC (Figure 2a, solid lines). To determine the degree of internalization, we used calicheamicin-unbound anti-CD33 antibody instead of GO, as described previously.[2] Four hours after the addition of the antibody, the amount of CD33 antigen on the cell surface decreased in all cell lines (Figure 2a, shaded curves), indicating that anti-CD33 antibody was internalized by all cell lines. Pretreatment with DAC did not induce any change in the degree of internalization of anti-CD33 antibody (Figure 2a), indicating that DAC has no promotive effect on the internalization of GO.

Next, given that free calicheamicin molecule number in cytoplasm is influenced by efflux pumps,[11] we then investigated whether DAC had any effect on one of these efflux pumps, multidrug resistance-associated protein 1 (MRP1). For this, MRP1 activity and mRNA expression were evaluated in the presence or absence of DAC treatment in K052, SKM-1 and Kasumi-3 cells. DAC treatment decreased the activity (Figure 2b) and the mRNA expression (Figure 2c) of MRP1 in K052 cells. This inhibition of MRP1 activity appears to be one of the causes of the enhancement of the effect of GO.

The last step in the activity of GO, namely the degradation of DNA by calicheamicin, was examined using the DNA ladder method (Figure 2d). GO was added to genomic DNA extracted from K052, SKM-1 and SKK-1 cells before and after DAC treatment.[10] In K052 and SKM-1 cells, the degree of fragmentation was more prominent in DAC pretreatment plus GO than in the control (DMSO plus GO), whereas no difference was seen in SKK-1 cells, indicating that DAC's enhancement of the effect of GO was partly due to the augmentation of calicheamicin's intercalation with DNA (Figure 2d).

Our present results clearly contrast with those of a previous phase III trial, the SWOG S0601 trial.[12] The major difference between studies is our use of pretreatment drugs, which retain cellular functions, rather than simultaneous use of strongly cytotoxic drugs. Most previous clinical trials of GO have aimed to escalate the cytotoxic intensity of treatment by simultaneous treatment of GO with conventional chemotherapy. The induction course in the SWOG S0106 trial for *de novo* AML used GO (6 mg/m^2) on the middle day (day 4) of a seven-day course of cytotoxic chemotherapy. Results showed no significant improvement in either complete remission rate or leukemia free survival, but rather a significant increase in deaths from early complications.[12] These findings might be interpreted two ways. First, the effect of GO might not have been sufficiently exerted owing to the inhibition of one or more cellular functions necessary for GO's action (Supplementary Figure S1) in leukemic cells by the preceding chemotherapy. Second, concurrent use of GO and chemotherapy might exacerbate bone marrow suppression, leading to the increase in death from complications.

Although GO was withdrawn from the US market based on the results of the SWOG S0106 trial, the MRC15 and ALFA studies recently reported that GO was beneficial for at least one or two subsets of *de novo* AML patients when used in low (3 mg/m^2 on day 1 in the MRC15 study) or fractionated doses (3 mg/m^2 three times on days 1, 4 and 7 in the ALFA study) in combination with chemotherapy.[13,14] These recent and the present findings argue strongly against the abandonment of GO, but rather for its re-evaluation for use in relapsed/refractory cases under a more sophisticated administration protocol.

In this study, we demonstrated that the combination of low-dose DAC followed by GO was effective in a part of relapsed/refractory AML cells. Our three major findings, namely that DAC showed the best compatibility with GO among the three epigenetic-modulating agents studied, that efficacy was optimized by pretreatment with DAC, and that DAC exerted this effect via an effect on efflux pumps and intercalation, will significantly assist the development of new and innovative protocols for the use of GO in patients with relapsed/refractory AML. Confirmation of the efficacy of this combination awaits validation in a large clinical trial.

CONFLICT OF INTEREST

The authors declare no conflict of interest.

ACKNOWLEDGEMENTS

We thank Dr M Ito for his critical reading of the manuscript.

M Kurimoto[1], H Matsuoka[2], N Hanaoka[1], S Uneda[1], T Murayama[3], T Sonoki[1] and H Nakakuma[1]
[1]*Department of Hematology/Oncology, Wakayama Medical University, Wakayama, Japan;*
[2]*Division of Medical Oncology/Hematology, Department of Medicine, Kobe University Graduate School of Medicine, Kobe, Japan and*
[3]*Department of Hematology, Hyogo Cancer Center, Akashi, Japan*
E-mail: matsuoh@med.kobe-u.ac.jp

REFERENCES

1 Giles F, Estey E, O'Brien S. Gemtuzumab ozogamicin in the treatment of acute myeloid leukemia. *Cancer* 2003; **98**: 2095–2104.
2 van Der Velden VH, te Marvelde JG, Hoogeveen PG, Bernstein ID, Houtsmuller AB, Berger MS *et al.* Targeting of the CD33-calicheamicin immunoconjugate Mylotarg (CMA-676) in acute myeloid leukemia: *in vivo* and *in vitro* saturation and internalization by leukemic and normal myeloid cells. *Blood* 2001; **97**: 3197–3204.
3 Leone G, Teofili L, Voso MT, Lubbert M. DNA methylation and demethylating drugs in myelodysplastic syndromes and secondary leukemias. *Haematologica* 2002; **87**: 1324–1341.
4 Lehmann U, Brakensiek K, Kreipe H. Role of epigenetic changes in hematological malignancies. *Ann Hematol* 2004; **83**: 137–152.
5 Graubert T, Walter MJ. Genetics of myelodysplastic syndromes: new insights. *Hematology Am Soc Hematol Educ Program* 2011; **2011**: 543–549.
6 Daskalakis M, Nguyen TT, Nguyen C, Guldberg P, Kohler G, Wijermans P *et al.* Demethylation of a hypermethylated P15/INK4B gene in patients with myelodysplastic syndrome by 5-Aza-2′-deoxycytidine (decitabine) treatment. *Blood* 2002; **100**: 2957–2964.
7 Issa JP, Kantarjian HM. Targeting DNA methylation. *Clin Cancer Res* 2009; **15**: 3938–3946.
8 Tang R, Faussat AM, Majdak P, Perrot JY, Chaoui D, Legrand O *et al.* Valproic acid inhibits proliferation and induces apoptosis in acute myeloid leukemia cells expressing P-gp and MRP1. *Leukemia* 2004; **18**: 1246–1251.
9 Insinga A, Monestiroli S, Ronzoni S, Gelmetti V, Marchesi F, Viale A *et al.* Inhibitors of histone deacetylases induce tumor-selective apoptosis through activation of the death receptor pathway. *Nat Med* 2005; **11**: 71–76.
10 ten Cate B, Samplonius DF, Bijma T, de Leij LF, Helfrich W, Bremer E. The histone deacetylase inhibitor valproic acid potently augments gemtuzumab ozogamicin-induced apoptosis in acute myeloid leukemic cells. *Leukemia* 2007; **21**: 248–252.
11 Walter RB, Raden BW, Hong TC, Flowers DA, Bernstein ID, Linenberger ML. Multidrug resistance protein attenuates gemtuzumab ozogamicin-induced cytotoxicity in acute myeloid leukemia cells. *Blood* 2003; **102**: 1466–1473.
12 Petersdorf S, Kopecky K, Stuart RK, Larson RA, Nevill TJ, Stenke L *et al.* Preliminary results of southwest oncology group study S0106: an international intergroup phase 3 randomized trial comparing the addition of gemtuzumab ozogamicin to standard induction therapy versus standard induction therapy followed by a second randomization to post-consolidation gemtuzumab ozogamicin versus no additional therapy for previously untreated acute myeloid leukemia. *Blood* 2009; **114**: (ASH Abstract, 790).
13 Burnett AK, Hills RK, Milligan D, Kjeldsen L, Kell J, Russell NH *et al.* Identification of patients with acute myeloblastic leukemia who benefit from the addition of gemtuzumab ozogamicin: results of the MRC AML15 trial. *J Clin Oncol* 2011; **29**: 369–377.
14 Castaigne S, Pautas C, Terre C, Raffoux E, Bordessoule D, Bastie J-N. Effect of gemtuzumab ozogamicin on survival of adult patients with de-novo acute myeloid leukaemia (ALFA-0701): a randomised, open-label, phase 3 study. *Lancet* 2012; **379**: 1508–1516.

Supplementary Information accompanies the paper on the Leukemia website (http://www.nature.com/leu)

MECHANISMS OF DEVELOPMENT 130 (2013) 195–206

Available at www.sciencedirect.com

SciVerse ScienceDirect

journal homepage: www.elsevier.com/locate/modo

TGF-beta-1 up-regulates extra-cellular matrix production in mouse hepatoblasts

Daisuke Sugiyama *, *Kasem Kulkeaw*, *Chiyo Mizuochi*

Division of Hematopoietic Stem Cells, Advanced Medical Initiatives, Department of Advanced Medical Initiatives, Kyushu University Faculty of Medical Sciences, Fukuoka 812-8582, Japan

ARTICLE INFO

Article history:
Received 30 January 2012
Received in revised form
9 September 2012
Accepted 15 September 2012
Available online 3 October 2012

Keywords:
TGF-beta-1
Matrix
Fetal liver
Hepatoblasts
Hematopoiesis

ABSTRACT

Fetal liver is the major embryonic hematopoietic organ and is extrinsically colonized by circulating hematopoietic stem cells (HSCs). Integrin beta-1 expression on HSCs is crucial for colonization, suggesting that interaction of Integrin beta-1 with extra-cellular matrix (ECM) factors promotes HSC adherence to fetal liver. However, little is known about how ECM production is regulated in fetal liver. Here we used flow cytometry to sort fetal liver compartments and detected ECM gene and protein expression predominantly in sorted hepatoblasts. mRNA and protein analysis suggested that TGF-beta-1 expressed by hepatoblasts, sinusoid endothelial cells and hematopoietic cells, binds to the TGF-beta receptor type-2 expressed on hepatoblasts to stimulate ECM production. Intra-cardiac injection of TGF-inhibitors into mouse embryos dramatically decreased fetal liver ECM gene expression. Taken together, our observations suggest that hepatoblasts predominantly produce ECM factors under control of TGF-beta-1 in fetal liver.

1. Introduction

In the mouse embryo, definitive hematopoiesis occurs in fetal liver, which consists of hepatoblasts expressing DLK-1 (Protein delta homolog 1), sinusoid endothelial cells expressing LYVE-1 (lymphatic vessel endothelial hyaluronic acid receptor 1) and hematopoietic cells expressing CD45 or Ter119 (Mouta Carreira et al., 2001; Tanimizu et al., 2003). In fetal liver hematopoietic stem cells (HSCs) undergo extensive self-renewal and differentiate into mature hematopoietic cells, particularly erythrocytes (Johnson and Jones, 1973; Johnson and Moore, 1975; Dzierzak et al., 1998; Ema and Nakauchi, 2000; Sugiyama and Tsuji, 2006). Both morphological observation and *in vitro* experiments suggest that fetal liver itself does not produce HSCs but is colonized by HSCs of extrinsic origin after 9.5 dpc (Johnson and Jones, 1973; Johnson and Moore, 1975; Houssaint, 1981; Cudennec et al., 1981). Previously, we demonstrated that circulating HSCs expressing c-Kit could colonize fetal liver (Sugiyama et al., 2005). Taken together, these data indicate that fetal liver provides instructive signals for HSC colonization, expansion and differentiation.

Integrin beta-1 is reportedly crucial for HSC colonization of fetal liver (Hynes and Yamada, 1982; Humphries et al., 1989; Hirsch et al., 1996; Frisch and Ruoslahti, 1997). Interaction of integrin heterodimers with extra-cellular matrix factors (ECMs) likely functions as a homing mechanism and enable HSCs and hematopoietic progenitor cells to reside in fetal liver (Patel and Lodish, 1987; Tsai et al., 1987; Long and Dixit, 1990; Williams et al., 1991; Long et al., 1992; Klein et al., 1993; Strobel et al., 1997). ECMs are produced in various cell

* Corresponding author. Address: Division of Hematopoietic Stem Cells, Advanced Medical Initiatives, Department of Advanced Medical Initiatives, Kyushu University Faculty of Medical Sciences, Station for Collaborative Research1 4F, 3-1-1 Maidashi, Higashi-Ku, Fukuoka 812-8582, Japan. Tel.: +81 92 642 6146/6210; fax: +81 92 642 6146.
E-mail address: ds-mons@yb3.so-net.ne.jp (D. Sugiyama).
0925-4773/$ - see front matter © 2012 Elsevier Ireland Ltd. All rights reserved.
http://dx.doi.org/10.1016/j.mod.2012.09.003

types and interact with cytokines to allow cells to interpret cytokine signaling in a particular context (Hynes and Yamada, 1982; Humphries et al., 1989; Frisch and Ruoslahti, 1997; Taipale and Keski-Oja, 1997).

In the current study, to determine which fetal liver component contributes to ECM production, we used flow cytometry to separate cells obtained from early fetal liver into hepatoblasts, sinusoid endothelial cells and hematopoietic cells, based on expression of surface molecules, and examined ECM expression in each component by real-time PCR, Western blot analysis and immunohistochemistry. Since Transforming Growth Factor (TGF)-betas are known to potentially regulate ECM production, we treated mouse embryos with their respective inhibitors and examined ECM gene expression in fetal liver (Nakamura et al., 1992; Ziyadeh et al., 1994; Chimal-Monroy and Diaz de Leon, 1999; Laping et al., 2002; Gaggioli et al., 2005). Overall, we observe that hepatoblasts predominantly produce ECM factors under control of TGF-beta-1 in fetal liver.

2. Materials and methods

2.1. Animals

ICR and C57BL/6J mice were purchased from Nihon SLC (Hamamatsu, Japan) and Kyudo (Tosu, Japan), respectively. *Map2k4*$^{+/-}$ mice were provided by RIKEN BioResource Center (Tsukuba, Japan). Noon of the day of the plug was defined as 0.5 day post-coitum (dpc). Embryos at 10.25, 11.5, 12.5 and 14.5 dpc were dissected in PBS under a stereomicroscope. Animals were handled according to Guidelines for Laboratory Animals of Kyushu University. This study was approved by the Animal Care and Use Committee, Kyushu University (Approval ID: A21-068-0).

2.2. Flow cytometry

For hematopoietic cells, circulating blood and fetal liver cells at 11.5 and 12.5 dpc were filtered through a 40 μm nylon mesh and washed once with PBS. Cells were stained with FITC-conjugated anti-mouse CD71 (BD Biosciences, San Diego, CA) or Integrin beta-1 (CD29) (BD Biosciences), PE-conjugated anti-mouse Sca-1 (BD Biosciences), PE-Cy7-conjugated anti-mouse CD45 (eBioscience, San Diego, CA), APC-conjugated anti-mouse c-Kit (BD Biosciences) and APC-Cy7-conjugated anti-mouse Ter119 (eBioscience) Abs. Cell sorting was accomplished using a FACS Aria cell sorter (BD, Franklin Lakes, NJ). For hepatoblasts and sinusoid endothelial cells, 12.5 dpc fetal liver was digested in 1 mg/mL collagenase (Washington Biochem Co., Freehold, New Jersey) in alpha-MEM containing 10% FBS, filtered through 40-μm nylon mesh, and washed once with PBS. Cells were stained with FITC-conjugated anti-mouse DLK-1 Ab (MBL, Nagoya, Japan), PE-conjugated anti-mouse LYVE-1 Ab (MBL), PE-conjugated anti-mouse Hepatocyte growth factor (HGF) receptor Ab (eBioscience), Alexa Fluor 647-conjugated anti-mouse E-cadherin Ab (eBioscience), biotin-conjugated anti-mouse TGF-beta receptor type-2 (TGFR-2) Ab (R&D Systems, Minneapolis, MN), APC-conjugated anti-mouse CD31 Ab (Biolegend, San Diego, CA), PE-Cy7-conjugated anti-mouse CD45 Ab (eBioscience), PE-Cy7-conjugated anti-mouse Ter119 Ab (eBioscience), and APC-Cy7-conjugated streptavidin (eBioscience).

2.3. Real-time PCR

RNA was extracted from both sorted and unsorted fetal liver samples, and cultured cells using a RiboPure™ kit (Life Technologies, Carlsbad, CA), and mRNA was reverse transcribed using a high-capacity RNA-to-cDNA kit (Life Technologies). cDNA quality was evaluated by PCR amplification of mouse *actin, beta (Actb)*. Thirty thermal cycles were used as follows: denaturation at 95 °C for 10 s, annealing at 60 °C for 20 s, and extension at 72 °C for 20 s. Gene expression levels were measured by real-time PCR with TaqMan® Gene Expression Master Mix and StepOnePlus™ real-time PCR (Life Technologies). All probes were from TaqMan® Gene Expression Assays (Life Technologies). All samples were assayed in triplicate wells. mRNA levels were normalized to *Actb* and the relative quantity (RQ) of expression was compared with a reference sample.

2.4. Western blot analysis

For Western blot analysis, protein was extracted from sorted cells using Qproteome® Mammalian Protein Prep Kit (QIAGEN). Lysates of whole fetal liver, sinusoid endothelial cells, hepatoblasts and hematopoietic cells were run on 12.5% SDS–polyacrylamide gels (Ready Gels J, Bio-Rad Laboratories, Hercules, CA) concurrently with a pre-stained protein marker (Precision Plus Protein™ Standards, Bio-Rad Laboratories) using Laemmle buffer. Gels were trans-blotted onto a PVDF membrane (Immobilon®-P Transfer Membrane, Millipore Billerica, MA). The membrane was blocked in 5% skim milk in TBS containing 0.1% Tween-20 (TBS-T) at 25 °C for 1 h, washed with washing buffer (TBS-T) and reacted with 1:5000 mouse anti-TGF-beta-1 monoclonal Ab solution (R&D systems), 1:200 anti-Fibronectin Ab (Santa Cruz Biotechnology, Santa Cruz, CA), 1:2000 anti-Vitronectin Ab (EPITOMICS, Burlingame, CA) or 1:1500 rabbit anti-Beta-actin Ab (IMGENEX, Sorrento Valley, CA) at 25 °C for 2 h. The membrane was then thoroughly washed and incubated in a solution of 1:1000 goat anti-mouse IgG-HRP conjugate (R&D systems) and 1:2500 goat anti-rabbit IgG-HRP conjugate (R&D systems) at 25 °C for 1 h. After washing, signals were visualized by soaking the membrane in substrate solution (Amersham™ ECL Plus Western Blotting Detection System, GE Healthcare, Buckinghamshire, UK). Images were captured using Chemi-Doc XRS (Bio-Rad Laboratories). Data were analyzed by Quantity One ver. 4.6.7 (Bio-Rad Laboratories) and displayed as intensity per mm^2.

2.5. Immunohistochemistry

Injected or uninjected ICR mouse embryos were fixed in 2% paraformaldehyde in PBS overnight at 4 °C and washed in PBS three times. After 27% sucrose infusion, embryos were embedded in OCT compound (Sakura Finetek, Tokyo, Japan) and frozen in liquid nitrogen vapor phase. Frozen embryos were sectioned at 20 μm, transferred onto glass slides (Matsunami, Osaka, Japan), and dried. After blocking in 1% BSA in

PBS, sections were incubated with primary antibodies overnight at 4 °C. After washing in PBS three times, sections were incubated with secondary antibodies and TOTO-3 (Life Technologies) for nuclear staining. Anti-mouse DLK-1 Ab (MBL), anti-Fibronectin Ab (Santa Cruz Biotechnology, Santa Cruz, CA), anti-Vitronectin Ab (EPITOMICS, Burlingame, CA), anti-mouse CD31 Ab (BD Bioscience), anti-rat beta1-integrin Ab (BD Bioscience), anti-mouse Lyve-1 Ab (MBL), anti-mouse c-Kit Ab (R&D Systems), and anti-human SMAD family member 3 (SMAD3) phospho Ser423/Ser42 Ab (EPITOMICS) served as primary antibodies and donkey anti-rabbit IgG-Alexa555, donkey anti-goat IgG-Alexa488 and Alexa568, donkey anti-rat IgG-Alexa488 (all from Life Technologies), rabbit anti-hamster IgG-Cy3 (Jackson ImmunoResearch Laboratories, West Grove, PA) were used as secondary antibodies. Coverslips were mounted with fluorescence mounting medium (Dako Corporation, Carpinteria, CA). Slides were observed using an FV-1000 confocal microscope (Olympus, Tokyo, Japan).

2.6. *Intra-cardiac injection*

TGF-beta receptor type-1 Kinase Inhibitor (Merck, Darmstadt, Germany) and TGF-beta receptor type-1 Kinase Inhibitor II (Merck) were dissolved in DMSO at 5 mg/mL. 0.2–0.5 μl of inhibitors, anti-TGF-beta-1 blocking antibody (MAB240, R&D systems) or mouse IgG Isotype control (MBL) were administered to 10.25 dpc ICR mouse embryos by intra-cardiac injection, as previously described (Sugiyama et al., 2003, 2005; Kulkeaw et al., 2009). As stated by the manufacture, the optimal inhibitor concentration (Primary Target IC50) is 51 nM in TGF-beta receptor type-1 Kinase Inhibitor, and 23 nM in TGF-beta receptor type-1 Kinase Inhibitor II, respectively. Embryos were isolated under a stereomicroscope (Leica Microsystems MZ6, Wetzlar, Germany) in PBS. Both the uterus and deciduo capsularis were removed and the yolk sac was cut along yolk sac arteries with care to avoid excessive hemorrhage. The amnion was opened to allow needle access to the heart. The injection needle was produced by pulling a glass capillary (Narishige GC-10, Japan) using a micropipette puller (Narishige, Tokyo, Japan). Injected embryos were immediately subjected to a mouse whole embryo culture system within 1 h of isolation.

2.7. *Mouse whole embryo culture*

Injected embryos were transferred to culture bottles containing 100% rat serum supplemented with 2 mg/ml glucose in a whole embryo culture system (Ikemoto Scientific Technology, Tokyo, Japan) and cultured for 6 or 12 h at 37 °C with a continuous supply of the gas mixture (60% O_2 and 5% CO_2 balanced with N_2) in the dark (Osumi-Yamashita et al., 1997). After whole embryo culture, embryos exhibiting no conspicuous bleeding or anomalies were analyzed for mRNA and protein expression. In addition, some fetal liver samples were isolated from embryos, pooled, filtered through a 40 μm nylon mesh, and their cell number counted.

2.8. *In vitro culture*

Hepatoblasts expressing DLK-1 were sorted from fetal liver at 12.5 dpc by flow cytometry, and 10,000 were cultured in 96-well plates with Opti-MEM (Life Technologies) containing 2% of fetal bovine serum in the presence or absence of TGF-beta-1 (10 ng/mL) (Wako, Osaka, Japan). After 6 h of culture, cells were collected and analyzed for mRNA expression.

3. Results

3.1. *Integrin expression on fetal liver hematopoietic cells*

Previously, it was reported that chimeric embryos generated with a component of *integrin beta 1 (Itgb1)*-deficient embryonic stem cells exhibited *Itgb1* null hematopoietic cells in the YS and blood, but not in fetal liver, suggesting that *Itgb1* is crucial for hematopoietic cell colonization of fetal liver (Hirsch et al., 1996). To confirm expression of Integrin beta-1 protein on hematopoietic cells, we first performed flow cytometry on blood and fetal liver cells obtained from 11.5 dpc mouse embryos. Integrin beta-1 was expressed on 94.9% of HSCs (CD45+/c-Kit+/Sca-1+) and 86.4% of erythroid cells (CD45−/Ter119+) in fetal liver, and on 96.8% of HSCs (CD45+/c-Kit+/Sca-1+) in circulation, whereas it was expressed on only 0.85% of circulating erythroid cells (CD45−/Ter119+) (Fig. 1A). Immunohistochemistry of fetal liver sections at 11.5 and 12.5 dpc showed that hematopoietic cells inside blood vessels surrounded by CD31-expressing endothelial cells did not express Integrin beta-1, while most hematopoietic cells outside blood vessels did, in agreement with flow cytometry data (Fig. 1B). To identify the alpha-chain partner of the beta-1-containing heterodimer, *integrin-alpha* expression was examined at stages ranging from HSCs to mature erythroid cells in mouse fetal liver using real-time PCR. As shown in Fig. S1, HSCs and various stages of differentiated erythroid cells were isolated by flow cytometry from fetal liver at 12.5 dpc based on expression of the cell surface markers Sca-1, c-Kit, CD71 and Ter119 (see Fig. S1 for a definition of lineage markers) (Suzuki et al., 2003; Inoue et al., 2011). When *integrin-alpha* expression was compared during erythropoiesis, *integrin alpha V (ItgaV)*, *Itga5*, *Itga6*, and *Itga9* mRNAs were predominantly expressed in HSC and hematopoietic progenitor cell fractions (Fig. 2A). No *integrin-alpha* expression was detected in the mature erythroid cell fraction (Sca-1−/c-Kit−/CD71−/Ter119+). When *integrin-alpha* expression was evaluated in each hematopoietic cell fraction, *Itga4* and *Itga6* were highly expressed in both HSC and BFU-E fractions, and *Itga4* was also expressed in relatively mature erythroid cells (Fig. 2B). Taken together, these observations imply that integrins expressed on both HSCs and hematopoietic progenitor cells interact with ECM binding partners, enabling cells to adhere properly to fetal liver.

3.2. *ECM factor expression in fetal liver*

To investigate the production of ECMs, we examined expression of several ECM genes in fetal liver at 12.5 and 14.5 dpc using real-time PCR. *Vitronectin (Vtn)* and *fibronectin1 (Fn1)* mRNAs were predominantly expressed in fetal liver (Fig. 3A). Morphological observation of fetal liver sections at 14.5 dpc revealed that hepatoblasts expressing DLK-1 were in close contact with HSCs and hematopoietic progenitor cells expressing c-Kit, implying that hepatoblasts may supply factors governing activities of HSCs and hematopoietic progeni-

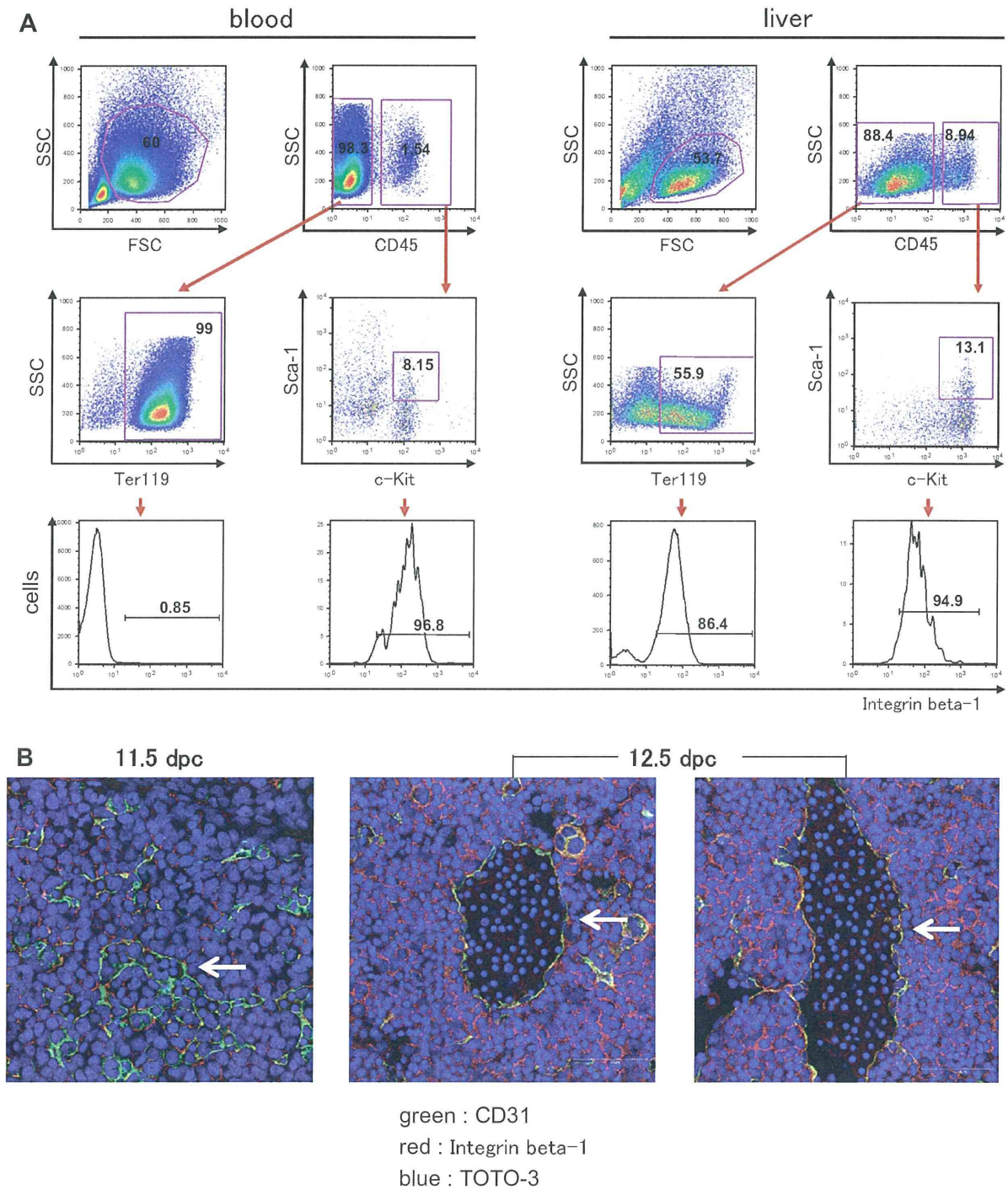

Fig. 1 – Integrin-beta-1 expression on hematopoietic cells in circulation and in fetal liver. (A) Samples were obtained from blood and fetal liver of ICR mouse embryos at 11.5 dpc. Expression of CD45 (common leukocyte antigen), Ter119 (glycophorin A), c-Kit (CD117, stem cell factor receptor), Sca-1 (stem cell antigen-1) and Integrin-beta-1 (CD29) was analyzed by flow cytometry. Integrin-beta-1 was expressed on 94.9% of HSCs (CD45+/c-Kit+/Sca-1+) and 86.4% of erythroid cells (CD45–/Ter119+) in fetal liver, and 96.8% of HSCs (CD45+/c-Kit+/Sca-1+) in circulation, whereas it was expressed on only 0.85% of erythroid cells (CD45-/Ter119+) in circulation. SSC and FSC define side scatter and forward scatter, respectively. (B) Liver sections were prepared from ICR mouse embryos at 11.5 dpc (Left) and 12.5 dpc (Middle and Right), stained with antibodies to CD31 (green) and Integrin-beta-1 (red) as well as TOTO-3 to identify nuclei, and observed under confocal microscopy. Arrows indicate that Hematopoietic cells inside blood vessels and surrounded by endothelial cells expressing CD31 do not express Integrin-beta-1, but most hematopoietic cells outside blood vessels do, in agreement with the data seen in (A). Original magnification was 20×.

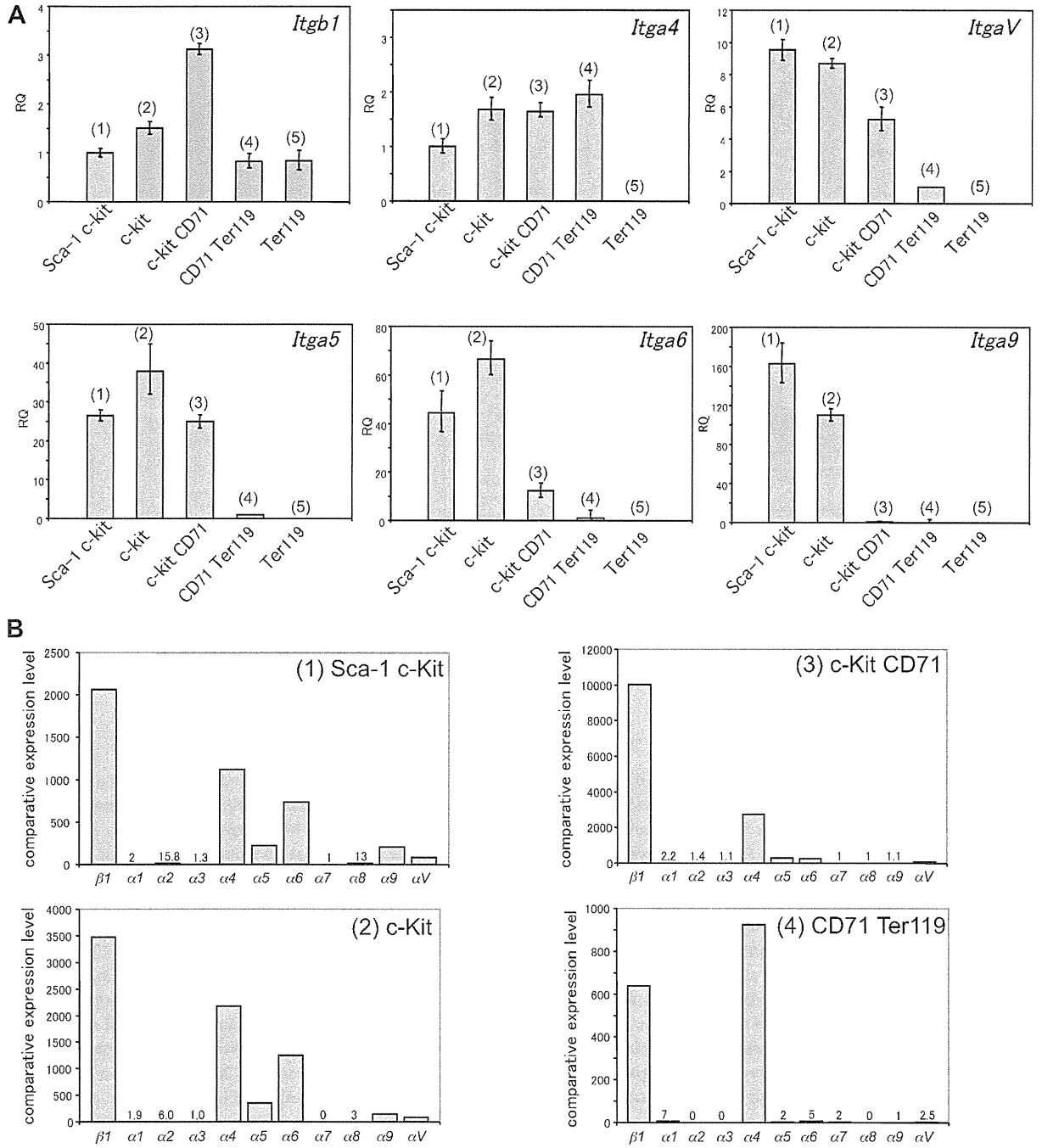

Fig. 2 – Integrin mRNA expression in fetal liver populations of the erythroid lineage. (A) HSCs and respective stages of differentiated erythroid cells were isolated from mouse fetal liver at 12.5 dpc based on expression of the cell surface molecules, Sca-1 (stem cell antigen-1), c-Kit (CD117, stem cell factor receptor), CD71 (transferrin receptor), and Ter119 (glycophorin A). Populations are defined as follows: (1) Sca-1+/c-Kit+, HSCs; (2) c-Kit+(Sca-1−/c-Kit+/CD71−/Ter119−), BFU-E; (3) c-Kit+/CD71+(Sca-1−/c-Kit+/CD71+/Ter119−), committed erythroid progenitors or CFU-E; (4) CD71+/Ter119+(Sca-1−/c-Kit−/CD71+/Ter119+), proerythroblasts; and (5) Ter119+(Sca-1−/c-Kit−/CD71−/Ter119+), mature erythroblasts and erythrocytes. Over 95% of defined HSCs expressed CD45 (common leukocyte antigen) (data not shown). Expression of *integrin-alpha* and *Itgb1* was examined in each cell fraction sorted by real-time PCR. RQ indicates relative quantification. *ItgaV*, *Itga5*, *Itga6*, and *Itga9* mRNAs were predominantly expressed in fractions (1) and (2). *Itga4* expression was not altered during erythroid cell differentiation. No expression of *integrin-alpha* was detected in fraction (5). (B) Comparison of expression levels of *integrin* genes in relatively differentiated erythroid cells is shown. Expression of *integrin-alpha* and *Itgb1* was examined by real-time PCR in each fraction of cells sorted according to gates defined in Supplementary Fig. S1. *Itga4* was expressed in fractions (3) and (4), which represent relatively mature erythroid cells.

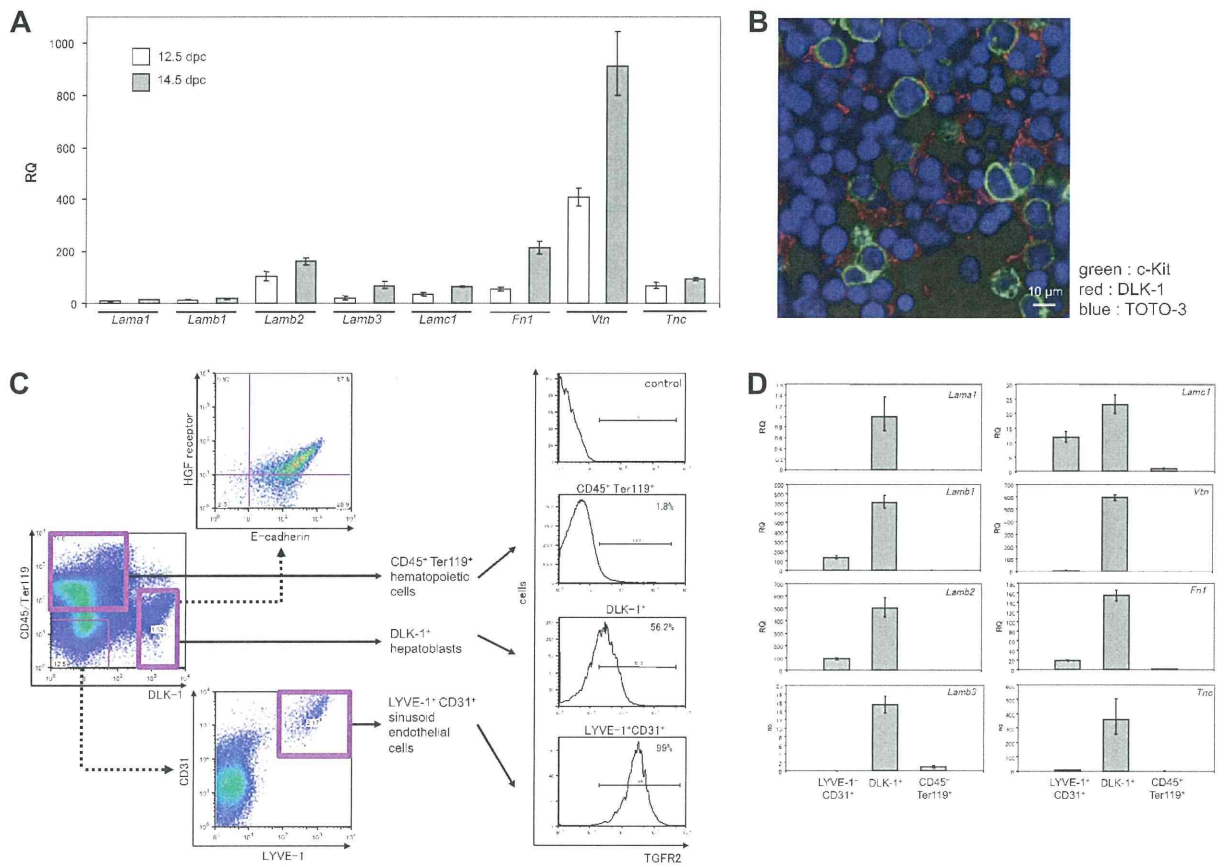

Fig. 3 – Separation of fetal liver components and expression of ECM factors. (A) Expression of *laminin, alpha 1 (Lama1)*, *laminin B 1 (Lamb1)*, *laminin, beta 2 (Lamb2)*, *laminin, beta 3 (Lamb3)*, *laminin, gamma 1 (Lamc1)*, *fibronectin 1 (Fn1)*, *vitronectin (Vtn)* and *tenascin C (Tnc)* was examined in fetal liver samples at 12.5 and 14.5 dpc by real-time PCR. Expression of *Vtn* and *Fn1* was predominantly seen in fetal liver. (B) Sections were prepared from ICR mouse embryos at 14.5 dpc, stained with antibodies to c-Kit and DLK-1, as well as TOTO-3 to define nuclei, and observed by confocal microscopy. Hepatoblasts expressing DLK-1 were in close contact with HSCs and hematopoietic progenitor cells expressing c-Kit. Original magnification was 40×. (C) A single cell fetal liver suspension was obtained at 12.5 dpc, and expression of CD45/Ter119, DLK-1, E-cadherin, HGF receptor, LYVE-1, CD31 and TGFR2 was analyzed by flow cytometry. (1) CD45−/Ter119−/DLK-1+ defines hepatoblasts; (2) CD45−/Ter119−/LYVE-1+/CD31+ defines sinusoid endothelial cells; and (3) CD45+/Ter119+ defines hematopoietic cells. 96.5% of hepatoblasts also expressed E-cadherin and 68.5% of them expressed HGF receptor, respectively. All CD45−/Ter119−/LYVE-1+ cells expressed CD31. TGFR2 was expressed in 1.8% of hematopoietic cells, 56.2% of hepatoblasts and 99% of sinusoid endothelial cells. (D) ECM expression was examined by real-time PCR in each fraction of cells sorted according to gate settings defined in (C). All ECM mRNAs were highly expressed in hepatoblasts. In particular, among ECMs, expression of *Lamb1*, *Lamb2*, *Vtn*, *Fn1* and *Tnc* was high in hepatoblasts compared to sinusoid endothelial cells and hematopoietic cells. (E) Liver sections were prepared from ICR mouse embryos at 12.5 dpc, stained as indicated with Fibronectin, Vitronectin and DLK-1 antibodies, as well as TOTO-3 (blue), and observed by confocal microscopy. DLK-1+ hepatoblasts expressed both Fibronectin and Vitronectin. Original magnification was 40×. (F) Vitronectin and Fibronection expression was examined by Western blot analysis in each fraction of cells sorted from ICR mouse fetal liver at 12.5 dpc, according to gate settings defined in (C). Protein expression levels were normalized to Beta-actin and displayed as intensity per mm^2. (G) Liver sections were prepared from wild-type (left panels) and *Map2k4*$^{-/-}$ (right panels) mouse embryos at 12.5 dpc, stained with Fibronectin (upper; red), Vitronectin (lower; red) and TOTO-3 (blue), and observed under confocal microscopy. Expression of Fibronectin and Vitronectin proteins was down-regulated in fetal liver of *Map2k4*$^{-/-}$ compared to wild-type mouse embryos. Original magnification was 20×.

tor cells (Fig. 3B). As shown in Fig. 3C, fractions of hepatoblasts, sinusoid endothelial cells and hematopoietic cells were isolated from mouse fetal liver at 12.5 dpc by flow cytometry based on the following markers: hepatoblasts, CD45−/Ter119−/DLK-1+; sinusoid endothelial cells, CD45−/Ter119−/LYVE-1+/CD31+; and hematopoietic cells, CD45+/Ter119+. We observed that 96.5% of hepatoblasts also expressed the hepatoblast marker E-cadherin. To investigate

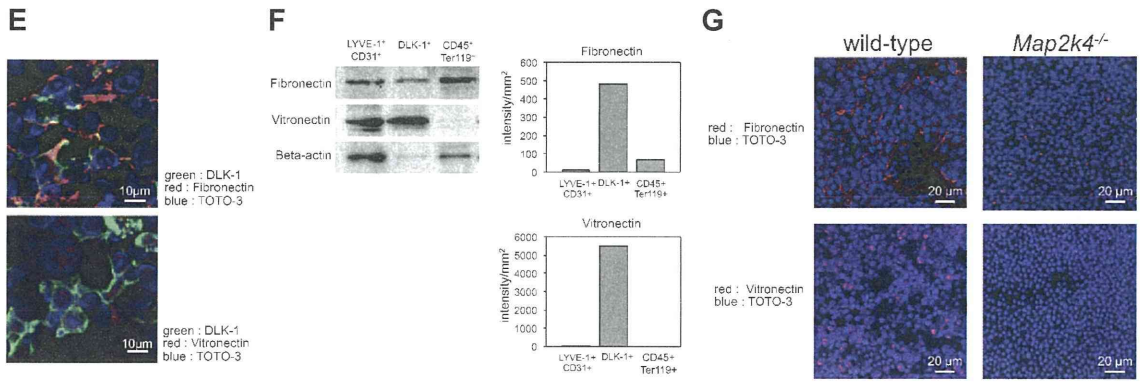

Fig. 3 – continued

which fetal liver component contributes to ECM-production, expression of genes encoding ECM factors was examined in hepatoblasts, sinusoid endothelial cells and hematopoietic cells by real-time PCR. All ECM genes analyzed, including *laminin B 1 (Lamb1)*, *laminin, beta2 (Lamb2)*, *Vtn*, *Fn1* and *tenascin C (Tnc)*, were highly expressed in hepatoblasts compared to sinusoid endothelial cells and hematopoietic cells (Fig. 3D). Both Fibronectin and Vitronectin were detected in fetal liver at 12.5 dpc by immunohistochemistry (Fig. 3E). In addition, Western blot analysis showed that hepatoblasts expressed Vitronectin and Fibronectin proteins at levels higher than those seen in sinusoid endothelial cells and hematopoietic cells (Fig. 3F). To characterize hepatoblast function in fetal liver, we analyzed *Map2k4* (*mitogen-activated protein kinase kinase* 4, formerly known as *Sek1* and *MKK4*)$^{-/-}$ mouse embryos, which lack fetal liver hepatoblasts (Nishina et al., 1997a, 1997b, 1999; Watanabe et al., 2002). Immunohistochemistry indicated that expression of Fibronectin and Vitronectin proteins was lower relative to that seen in wild-type mouse embryos in fetal liver of *Map2k4*$^{-/-}$ mouse embryos (Fig. 3G). Both mRNA and protein expression data and analysis of mutant embryos suggest that hepatoblasts expressing DLK-1 are primarily responsible for ECM production in fetal liver.

3.3. *Regulation of ECM production by TGF-beta-1*

We next asked how ECM production in hepatoblasts is regulated. Based on findings suggesting that TGF-betas and HGF regulate ECM production (Nakamura et al., 1992; Ziyadeh et al., 1994; Chimal-Monroy and Diaz de Leon, 1999; Laping et al., 2002; Gaggioli et al., 2005), we analyzed gene expression of *Tgfb1*, *Tgfb2*, *Tgfb3* and *Hgf* in whole fetal liver samples at 12.5 and 14.5 dpc (Fig. 4A). *Tgfb1* was predominantly expressed in fetal liver at both stages. TGF-beta-1 protein was also detected by Western blot analysis in fetal liver at 12.5 dpc (Fig. 4B). To investigate whether TGF-beta-1 and HGF signals regulate ECM production in fetal liver, we used real-time PCR to examine expression of *Tgfb1* and *Tgfbr2*, which encodes the TGF-beta receptor type 2 (TGFR-2), and *Hgf* and *Met*, which encodes HGF receptor, in hepatoblasts, sinusoid endothelial cells and hematopoietic cells. *Tgfb1* was predominantly expressed in sinusoid endothelial cells and hematopoietic cells, whereas *Tgfbr2* was predominantly expressed in both sinusoid endothelial cells and hepatoblasts (Fig. 4C). Western blot analysis showed that TGF-beta-1 protein was highly expressed in both hepatoblasts and sinusoid endothelial cells (Fig. 4D). *Tgfb1* and *Tgfbr2* expression was detected in HSCs and at each stage of differentiated erythroid cells isolated from fetal liver at 12.5 dpc (Fig. S2). By contrast, both *Hgf* and *Met* were predominantly expressed in hepatoblasts. Flow cytometric analysis also showed that TGFR-2 and HGF receptor proteins were expressed in 56.2% and 68.5% of hepatoblasts, respectively (Fig. 3C).

To further investigate which signal functions in ECM production, TGFR2 inhibitors were administered to mouse embryos using an intra-cardiac injection technique that we developed for use in 10.0–10.5 dpc embryos (Sugiyama et al., 2003, 2005; Sasaki et al., 2010). After hepatoblasts develop in fetal liver, circulating hematopoietic cells home to fetal liver after 9.5 dpc (Johnson and Jones, 1973; Johnson and Moore, 1975; Houssaint, 1981; Cudennec et al., 1981; Sugiyama et al., 2005). To rule out effects of ECM gene expression by hematopoetic cells (Fig. 3D), we chose to inject inhibitors at 10.25 dpc, when fetal liver is predominantly comprised of hepatoblasts. Following injection, we maintained embryos for variable time periods in a whole embryo culture system (Osumi-Yamashita et al., 1997; Kulkeaw et al., 2009). Twelve hours after injection of a specific, cell-permeable TGF-beta receptor type-1 Kinase Inhibitor, *Vtn*, *Fn1* and *Tnc* expression levels were down-regulated relative to controls (Fig. 5A). Injection of a different TGF-beta receptor type-1 Kinase Inhibitor II promoted a detectable decrease in *Vtn* expression by 6 h of culture and significant decreases in *Vtn*, *Fn1* and *Tnc* expression levels relative to controls after 12 h of culture (Fig. 5B). TGF-beta receptor type-1, also known as ALK5, binds to both growth differentiation factor-1 (GDF1) and TGF-betas. To determine whether down-regulation of ECM genes resulted from specific alterations in TGF-beta-1 signaling, anti-TGF-beta-1 blocking antibody was injected into mouse embryos. As shown in Fig. 5C, *Vtn*, *Fn1* and *Tnc* expression was down-regulated after 12 h of whole embryo culture. To confirm that TGF-beta-1 signaling is down-regulated after administration of anti-TGF-beta-1 blocking antibody, injected embryos were stained with anti-phosphorylated SMAD3 antibody. A 19.4% decrease in SMAD-phosphorylation was observed after injection of

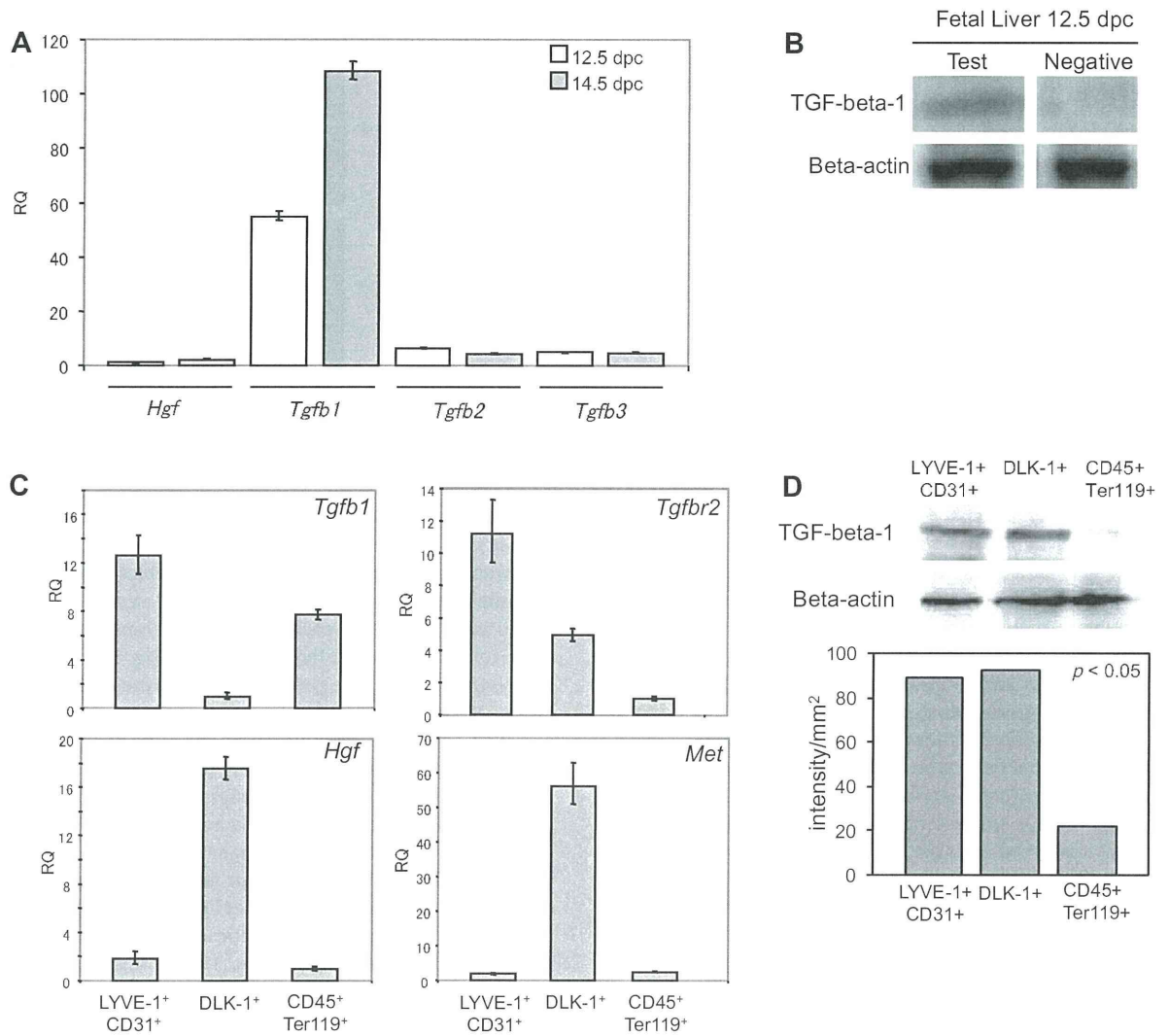

Fig. 4 – TGF-beta and HGF expression in fetal liver. (A) Expression of *Tgfb1*, *Tgfb2*, *Tgfb3* and *Hgf* was examined in fetal liver samples at 12.5 and 14.5 dpc. *Tgfb1* was highly expressed at both stages. (B) TGF-beta-1 protein was detected by Western blot analysis of fetal liver at 12.5 dpc. (C) Expression of *Tgfb1* and *Tgfbr2*, which encodes its receptor, and *Hgf* and *Met*, which encodes its receptor, was examined by real-time PCR in hepatoblasts, sinusoid endothelial cells and hematopoietic cells according to gates defined in Fig. 3C. *Tgfb1* was predominantly expressed in sinusoid endothelial cells and hematopoietic cells, whereas *Tgfbr2* was highly expressed both in sinusoid endothelial cells and hepatoblasts. Both *Hgf* and *Met* were highly expressed in hepatoblasts. (D) TGF-beta-1 expression was examined by Western blot analysis in each fraction of cells sorted from ICR mouse fetal liver at 12.5 dpc according to gate settings defined in Fig. 3C. Protein expression levels were normalized to Beta-actin and displayed as intensity per mm^2.

anti-TGF-beta-1 blocking antibody (Fig. S3). As shown in Fig. S4, some DLK-1 positive and negative cells were stained with anti-phosphorylated SMAD3 Ab in fetal liver at 10.5 dpc. Taken together, it is likely that TGF-beta-1 signaling in both hepatoblasts expressing DLK-1 and non-hepatoblasts was down-regulated after administration of anti-TGF-beta-1 blocking antibody.

To further investigate how TGF-beta-1 controls ECM production in hepatoblasts, we sorted hepatoblasts expressing DLK-1 and cultured them in the presence of TGF-beta-1. After 6 h of culture, *Vtn*, *Fn1* and *Tnc* expression was up-regulated (Fig. 5D). Taken together, these data strongly suggest that TGF-beta-1/TGFR-2 signaling promotes ECM production by hepatoblasts in fetal liver.

4. Discussion

Hepatoblasts were originally regarded as common progenitors of hepatocytes and biliary epithelial cells and thought to support liver construction through formation of a mesh-like structure (Tanimizu et al., 2003; Sasaki and Sonoda, 2000). Recently, it was reported that expression of SCF and EPO by

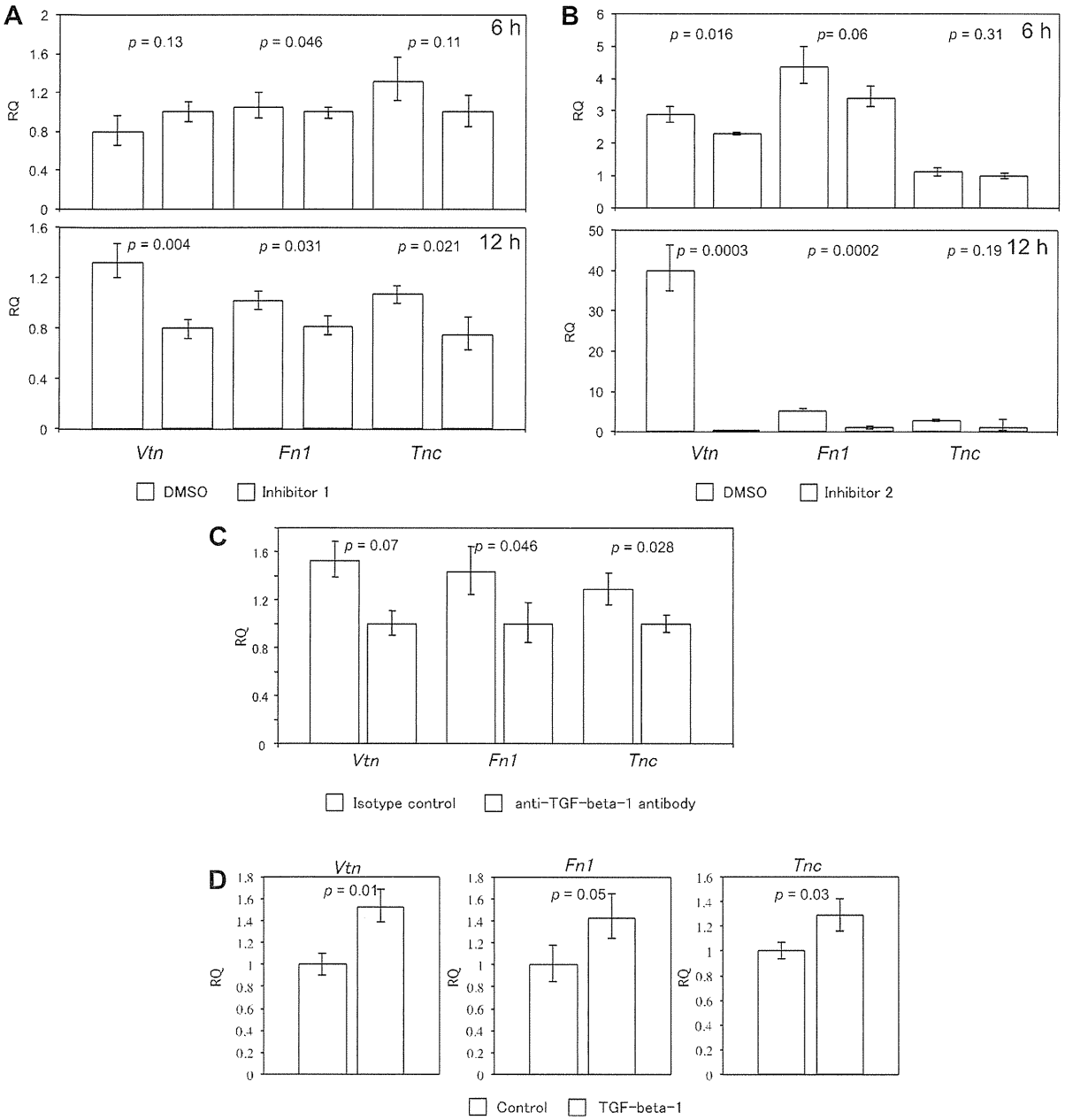

Fig. 5 – Functional analysis of the effect of TGF-beta-1/TGFR2 signaling on ECM production in fetal liver. (A) A TGF-beta receptor type-1 Kinase Inhibitor (inhibitor 1) was administered to ICR mouse embryos at 10.25 dpc by intra-cardiac injection, and embryos were then cultured in a whole embryo culture system. Left and right bars show control (DMSO injection) and sample (inhibitor injection) responses, respectively. Expression of *Vtn*, *Fn1* and *Tnc* genes was slightly down-regulated after 6 h and then more significantly so at 12 h of whole embryo culture compared to controls. (B) TGF-beta receptor type-1 Kinase Inhibitor II (inhibitor 2) was administered as in (A). Expression of *Vtn*, *Fn1* and *Tnc* was slightly and then significantly down-regulated relative to controls after 6 and 12 h of whole embryo culture, respectively. (C) Anti-TGF-beta-1 blocking antibody was administered as in (A). Left and right bars show control (Isotype IgG injection) and sample (blocking antibody injection), respectively. Expression of *Vtn*, *Fn1* and *Tnc* was down-regulated after 12 h of whole embryo culture. (D) Hepatoblasts expressing DLK-1 were sorted from 12.5 dpc fetal liver by flow cytometry and 10,000 cells were cultured with or without TGF-beta-1 (10 ng/mL). *Vtn*, *Fn1* and *Tnc* expression was up-regulated after 6 h of *in vitro* culture with TGF-beta-1.